STRAIN ENERGY BASED FATIGUE MODEL FOR NOTCHED PART SUBJECTED TO MULTIAXIAL LOADING

by

Cumali Özgür Karadeniz

B.S., Mechanical Engineering, Boğaziçi University, 2010

Submitted to the Institute for Graduate Studies in
Science and Engineering in partial fulfillment of
the requirements for the degree of
Master of Science

Graduate Program in Mechanical Engineering
Boğaziçi University

2013

This study is dedicated to most important person in my life, Merve Ayça Telemez. Fifty years after from now also, I wish you to be in my life. I am sure you will be beautiful as you are today.

ACKNOWLEDGEMENTS

I should first indicate how I am grateful to my family due to their infinite patience, love and support for me. Even only their existence was a big motivation for me to finish this study. My mother Gülizar Karadeniz, my father İrfan Karadeniz and my brother Deniz Karadeniz are the persons in my life that I clearly know they will be with me no matter what happens. I hope that I can be a great son and brother, and they will proud of me; this is what they deserve.

I would like to express my gratitude to my thesis supervisor, Prof. Fazıl Önder Sönmez, for his leadership, time, care and favor. Without his support, it is clear that I could not succeed. I am very honored and happy to have a chance to study with him. From now on, I hope I can succeed to make him proud of me at the end.

I also thank to the committee members, Assoc. Prof. Bülent Ekici and Assoc. Prof. Nuri Ersoy. Their comments and suggestions mean a lot to me.

I also grateful to my friend Sedat Aksu. His immense knowledge and helpful personality was a big motivation for me.

And lastly, I would like to thank the sense of my life, Merve Ayça Telemez. I cannot explain the part of her in this study, as in my life, even roughly.

ABSTRACT

STRAIN ENERGY BASED FATIGUE MODEL FOR NOTCHES SUBJECTED TO MULTIAXIAL LOADINGS

In this study, a new fatigue assessment model is developed for high cycle fatigue of metals under multiaxial proportional loading. The proposed model uses readily available material properties and contains no parameters depending on geometry or loading conditions. It is applicable to parts containing a notch or locally high stressed regions. The effects of loading conditions and geometry are taken into consideration via the use of equivalent strain energy density parameter introduced in this study. Its numerical value depends on the strain state within the part obtained through finite element analysis. The predictions of the proposed fatigue model are compared with the results of two experimental studies conducted on specimens with different notch geometries, fillet and hole, and on two different steel materials; one was a carbon steel, the other was a stainless steel. In the experiments, different types of multiaxial loads were applied; one was bending combined with torsion, the other was axial load combined with torsion. For these different conditions, the model predictions and the experimental results correlate quite well.

ÖZET

ÇOK YÖNLÜ YÜKLEMEYE MARUZ KALAN ÇENTİKLİ YÜZEYLER İÇİN GERİLİM ENERJİSİ BAZLI YORULMA MODELİ

Bu çalışmada, orantılı çok yönlü yükleme altındaki yüksek yorulma ömürlü metaller için yeni bir yorulma modeli geliştirilmiştir. Önerilen model, herhangi bir geometri ve yük factöründen bağımsız, çentikli veya kısmı yüksek gerilme bölgesine sahip parçalar için, tamamen mevcut malzeme özelliklerini kullanır. Yükleme koşulları ve geometrik etkenler ilk defa bu çalışmada giriş yapılan eşdeğer gerilim enerji yoğunluğu vasıtası ile dikkate alınmıştır. Eşdeğer gerilim enerji yoğunluğunun değeri, sonlu elemanlar analizi ile belirlenen kısımdaki gerilim durumuna bağlıdır. Önerilen yorulma modelinin sonuçları iki farklı deney sonucu ile karşılaştırılmıştır. Deneylerdeki malzemeler çentikli olup, birinde kavis tipi çentik diğerinde ise delik bulunmaktadır. Kullanılmış malzemeler ise, birinde karbon çeliği diğerinde paslanmaz çeliktir. Deneylerde parçalara etki eden yükler, birinde eğilme ve burulmanın kombinasyonu, diğerinde ise eksenel yükleme ve burulmanın kombinasyonudur. Bu farklı koşullarda, yorulma modelinin tahminleri ile deneysel sonuçlar iyi derecede uyumludur.

TABLE OF CONTENTS

LIST OF FIGURES

LIST OF TABLES

LIST OF SYMBOLS

b	Axial fatigue strength exponent
b'	Shear fatigue strength exponent
c	Axial fatigue ductility exponent
c'	Shear fatigue ductility exponent
D	Damage parameter
G	Shear modulus
H_v	Heaviside function
J	Polar moment of inertia
K	Strain hardening coefficient
K'	Cyclic strength coefficient
n	Strain hardening exponent
N_f, $2N_f$	Number of cycles to failure, Number of reversals to failure
R	Proportionality constant
S_y	Yield strength
S_u	Ultimate strength
T	Applied torque
U	Strain energy density (elastic, plastic, total, alternating, threshold, equivalent or element base strain energy density depending on the subscripts and/or superscripts)
V	Volume (material or element base volume depending on the subscripts and/or superscripts)
α	Crack length
γ	Shear strain
γ_f'	Shear fatigue ductility coefficient
ε	Strain (elastic, plastic, total, alternating, mean, Von-Mises equivalent, necking or normal strain depending on the subscripts and/or superscripts)
ε_f'	Axial fatigue ductility coefficient

E	Elastic modulus
θ	Twist angle
ν	Poisson's ratio
σ	Stress (elastic, plastic, total, alternating, mean, Von-Mises equivalent, hydrostatic, reference, necking, normal stress or fatigue limit depending on the subscripts and/or superscripts)
σ_f'	Axial fatigue strength coefficient
τ	Shear stress
τ_f'	Shear fatigue strength coefficient
φ	Twist angle per unit length
ϕ	Biaxial stress ratio
$\Psi(N_f)$	Function of asymmetry sensitivity

LIST OF ACRONYMS/ABBREVIATIONS

2D	Two Dimensional
3D	Three Dimensional
APDL	Ansys Parametric Design Language
CDM	Continuum Damage Mechanics
FE	Finite Element
FEA	Finite Element Analysis
FEM	Finite Element Modeling
HCF	High Cycle Fatigue
MSC	Microstructurally Short Crack
PSC	Physically Short Crack

1. INTRODUCTION

Load carrying members in mechanical structures are usually subjected to cyclic loads that eventually lead to fatigue fracture. Accurate fatigue assessment models are needed during the design of such parts to ensure their safety. Fatigue life highly depends on the type of material geometry of the part and loading conditions. A model should correctly account for these effects. Beside accuracy, a model should be applicable to a wide range of parts having different geometries and subjected to different loading conditions. Apart from generality, a practicable model should require a low number of experimentally determined coefficients and experiments need not be repeated for different geometries and loading conditions.

Engineering structures usually contain notched parts. The notch may be fillet, hole, groove, chamfer, or any irregular shape which acts as a stress raiser. These may significantly reduce fatigue life of a part. Fatigue models account for the effect of notches by introducing fatigue stress concentration factors or notch factors. These factors highly depend on geometry and their values are available only for common geometries and standard shapes like circular fillets, holes, circular grooves and bolt threads. Consequently, the available models are applicable only to a small fraction of mechanical parts. For a part with a freeform shape, there is no reliable method to predict the fatigue life without experimentally determining the notch factor. Although, models [1-7] were developed for notched parts, they all use experimentally determined notch factors. Another factor to be considered is the loading state. Unlike laboratory specimens, mechanical parts may be subjected to quite complex multiaxial loads. Notch area is typically subjected to multiaxial state, even if the loading is uniaxial [1]. A model should correctly account for any possible stress state without resorting to empirical load factors. In a typical industrial design process, various geometries are tried, the corresponding performances are estimated using suitable models, and then the best design is chosen to make prototypes. If the part has nonstandard or irregular shape and fatigue failure is the critical mode, this approach cannot be adopted because the predictions of the available fatigue models will be unreliable. The design process will then involve extensive experiments, educated guesses, and trial-and-error. Shape and topology optimization methods, which have been gaining widespread use

in the industrial design procedures, can never be applied, if the fatigue life needs to be evaluated in each iteration.

This study focuses on high cycle fatigue (HCF) where industrial parts mostly fall into this category with a fatigue lifetime longer than 10^3 cycles. The study also aims to develop a fatigue assessment model that can accurately predict fatigue life of nonstandard and irregularly shaped mechanical parts under general multiaxial loading conditions without relying on load or geometry factors. This is achieved by introducing equivalent strain energy density. This parameter is computed using the strain energy density distribution within the part. Although, similar concepts were developed before like equivalent stress and equivalent strain, they are calculated for the most critical point. For this reason, use of those parameters yields highly nonconservative results for notched parts.

2. FATIGUE ASSESSMENT MODELS

In this chapter a review of fatigue assessment models is given. They are classified in three major groups. One is damage mechanics combined with critical plane approach, the other is energy based models and the last one is fracture based models. Considering the aim of this study, the classification is done not on whether the model is stress or strain based, but on the parameterization in the model.

2.1. Damage Mechanics and Critical Plane Approaches

In this category, fatigue models related with damage mechanics and critical plane approach will be outlined. The idea of the damage mechanics approach simply states that fatigue life of a material is related to a term called damage in the material. If the damage of the specimen is high, remaining fatigue life or simply remaining number of cycle to the failure is then low. Computation methodology of damage in the material and the relation between damage and remaining fatigue life define the variety of such models. Critical plane approaches develop fatigue models which calculates the response of the material to certain load condition in a specific region. This idea states that stress, strain or any other material response which lies on a specific plane and/or with specific direction determine and contribute to the fatigue life.

Chaboche provided a relation between remaining fatigue life of a material and a damage parameter [8, 9]. The way of doing this is so called Continuum Damage Mechanics (CDM) which requires;

- Definition of damage, its features and the relation between the main mechanical properties and the microstructural damage level of material.
- The equations and formulation for the damage parameters by the help of thermodynamic aspects.

The main idea of the CDM method may be formulized as [8, 9]

$$\frac{N_2}{N_f} = 1 - D = 1 - \frac{N_1}{N_f} \tag{2.1}$$

where N_1 and N_2 are spent fatigue life and remaining fatigue life, respectively, N_f total fatigue life and D is damage parameter corresponds to damage state of the material. Obviously, D is initially equal to 0 and it is equal to 1 at the final state, where material fails. The author also provides more physical relation between D and stress parameters:

$$\tilde{\sigma} = \frac{\sigma}{1 - D} \tag{2.2}$$

where $\tilde{\sigma}$ is effective stress, which is the stress level of undamaged material and σ is the stress in damaged material.

CDM also uses thermodynamics aspect to relate this damage parameter with the strain energy parameters such that

$$dU_e = \sigma d\varepsilon_e \tag{2.3}$$

$$-Y = \frac{U_e}{1 - D} \tag{2.4}$$

$$-Y = \frac{\sigma_{eq}^2}{2E(1-D)^2}\left[\frac{2}{3}(1+\nu) + 3(1-2\nu)\left(\frac{\sigma^H}{\sigma_{eq}}\right)^2\right] \tag{2.5}$$

where U_e is the elastic strain energy density, ε_e elastic strain, $-Y$ is the elastic strain energy release rate, σ_{eq} is Von-Mises equivalent stress, E is the elastic modulus, ν is Poisson's ratio and σ^H is hydrostatic stress.

Furthermore, Marco and Starkey [10] presented a fatigue damage accumulation model, which was modified by Monson [11] also. A general formula was attained as

$$dD = D^{\alpha_1(\sigma_{max},\tilde{\sigma})}\left[\frac{\sigma_{max}-\tilde{\sigma}}{M(\tilde{\sigma})}\right]^{\beta_1} dN_f \tag{2.6}$$

where α_1 is a function for which several candidate forms are presented by Chaudonneret and Chaboche [3], σ_{max} is the maximum stress, M is a function that needs to be deduced from a linear dependency between $\tilde{\sigma}$ and fatigue limit, β_1 is a material parameter and N_f is the fatigue life.

Xiao *et al.* [12] presented a CDM model for high-cycle fatigue using the definitions given in previous studies [8, 9]. The relation between damage parameter and fatigue life, in other words number of cycles to failure, was presented as

$$\frac{dD}{dN_f} = \frac{\overline{B}}{q(1-D)^{2q}} \frac{(1-R^{2q})}{\left(\frac{1}{2}(1-R)\right)^{2q}} \sigma_{eqa}^{2q} \qquad 0 \le R < 1 \tag{2.7}$$

where R is the ratio of minimum equivalent stress to maximum equivalent stress, σ_{eqa} is equivalent stress amplitude, $\bar{B}$ and q are material and geometry based parameters that need to be determined experimentally. The case where $R < 0$ can be found in [12]. After integration from $D = 0$ to $D = 1$, one obtains

$$N_f = \frac{q\left(\frac{1}{2}(1-R)\right)^{2q}}{(2q+1)\overline{B}(1-R^{2q})} \sigma_{eqa}^{-2q} \tag{2.8}$$

Authors first presented this equation for uniaxial case by considering the sign effect of R. However, Equation 2.8 is written for general multiaxial case and R is always positive when equivalent stresses are used.

The main disadvantage of using Equation 2.8 is that it needs empirical parameters, $\bar{B}$ and q, which depend on material, geometry and loading conditions that need to be determined in every case for irregularly shaped geometries. The authors provided the

values for an aluminum alloy, 7075-T6. The results showed a good correlation with experimental results.

Dattoma *et al.* [13] developed a fatigue damage model, very similar to the one proposed by Xiao *et al.* [12]. The fatigue life of the material was given as

$$N_f = \frac{1}{1-\alpha_2}\frac{1}{1-\beta_2}\left(\frac{\sigma_{eqa}}{M_0}\right)^{-\beta_2} \tag{2.9}$$

where α_2, β_2, and M_0 are damage model parameters, and α_2 is defined as

$$\alpha_2 = 1 - \frac{1}{H}\langle\frac{\sigma_{eqa}-\sigma_f}{S_u-\sigma_{eqa}}\rangle^a \tag{2.10}$$

where α and H are model and material parameters that need to be determined experimentally, σ_f is fatigue limit, S_u ultimate strength and operator $\langle X\rangle$ is defined as $\langle X\rangle = 0$ if $X \leq 0$ and $\langle X\rangle = X$ if $X > 0$.

Giancane *et al.* [4] extended the previous study [13] to notched components. Using the same material properties and damage parameters, the fatigue limits of two notched specimens were estimated and compared with experimental results. The disadvantage of using this model in a design is that the fatigue limit depends on the geometry.

Shang and Yao [14] presented a fatigue damage model which took into account fatigue limit, mean stress, damage and loading parameters with the same idea introduced in [4, 12, 13]. The model can be extended to multiaxial loadings by replacing uniaxial stress and strain components with the relevant equivalent stress and strain values.

In contrast to the models in [4, 12, 13], this model [14] uses the true stress-true strain relation. The stress based formulation was given as

$$N_f = \alpha_2 M_0^{\beta_2} \ln\left(\sigma_{eqa} - \sigma_{f_{-1}}\left(1 - b_{sy}\sigma_{eqm}\right)\right)\left[\frac{\sigma_{eqa}}{1-b'_{sy}\sigma_{eqm}}\right]^{-\beta_2} \tag{2.11}$$

where $\sigma_{f_{-1}}$ is the fatigue limit for fully reversed loading, σ_{eqm} is equivalent stress mean, b_{sy} and b'_{sy} are model parameters. The strain based relation can be obtained by using strain-hardening rule as

$$\sigma_{eqa} = K(\varepsilon_{eqa})^n \tag{2.12}$$

$$N_f = \alpha_2 M_0^{\beta_2} \frac{\ln\left(K(\varepsilon_{eqa})^n - \sigma_{f_{-1}}(1 - b_{sy}\sigma_{eqm})\right)}{H_v\left(K(\varepsilon_{eqa})^n - \sigma_{f_{-1}}(1 - b_{sy}\sigma_{eqm})\right)} \left[\frac{K(\varepsilon_{eqa})^n}{1 - b'_{sy}\sigma_{eqm}}\right]^{-\beta_2} \tag{2.13}$$

where ε_{eqa} is equivalent strain amplitude, K and n are strain-hardening coefficient and exponent, respectively, and H_v is Heaviside function defined as $H_v(x) = 0$ if $x \leq 0$ and $H_v = 1$ if $x > 0$.

The authors [14] compared the results with experimental data for normalized 45 steel and 16 Mn steel. However, only the values of α_2 was presented for both materials which were 0.0421 and 0.0416, respectively.

All of the above fatigue damage models are based on stress and/or strain response. However, Chen *et al.* [15] introduced a fatigue damage model based on critical plane approach. The objective to determine the critical plane under multiaxial loading based on axial strain parameter or shear strain parameter depending on which one is larger. Number of cycles to failure was found using Coffin-Manson-Basquin relations as

$$\varepsilon_{eqa}^{cr} = \frac{\sigma'_f}{E}(2N_f)^b + \varepsilon'_f(2N_f)^c \quad \text{for axial loading} \tag{2.14}$$

$$\gamma_{eqa}^{cr} = \frac{\tau'_f}{E}(2N_f)^{b'} + \gamma'_f(2N_f)^{c'} \quad \text{for torsional loading} \tag{2.15}$$

where ε_{eqa}^{cr} and γ_{eqa}^{cr} are critical axial and shear equivalent strain amplitudes, σ'_f and τ'_f are axial and shear fatigue strength coefficients, ε'_f and γ'_f are axial and shear fatigue ductility coefficients, b and b' are axial and shear fatigue strength exponents, c and c' are axial and shear fatigue ductility exponents, respectively. If the axial damage is higher than shear damage, then critical axial strain amplitude should be used to predict the fatigue life of the

material. Similarly, if the shear damage is higher, then critical shear strain formula, Equation 2.15, is used. The critical axial and shear strain amplitudes are calculated as follows if the maximum normal strain relief and maximum shear strain are known.

$$\varepsilon_{eqa}^{cr} = \sqrt{\varepsilon_n^{*2} + 1/3(\Delta\gamma_{max})^2} \tag{2.16}$$

$$\gamma_{eqa}^{cr} = \sqrt{\varepsilon_n^{*2} + (\Delta\gamma_{max})^2} \tag{2.17}$$

where ε_n^* is maximum normal strain relief between adjacent turning points of the maximum shear strain on the critical plane and γ_{max} is maximum shear strain. The model was compared with the experimental results AISI 304, SNCM630, S460N, A533B, Inconel 718 and S45C materials. The results are presented for the cases of fully axial strain based, fully shear strain based and competitive between axial and shear strain based which is an average of those with different weight fraction as discussed in this study. The results show that, making decision between axial and shear strain parameter increases the confidence level.

Brown and Miller [16] introduced a multiaxial critical plane approach in order to assess a fatigue model where the critical plane is the maximum shear plane. The model proposes a crack propagation dominant fatigue prediction. In order to control the each state of strain, a plot of maximum shear strain amplitude and tensile strain amplitude is illustrated. Although the model is an essential reference for multiaxial critical plane approaches, it needs experimental studies.

Ninic [17] developed a stress based fatigue model for high cycle fatigue and compared this model with the models proposed by McDiarmid [18, 19] and, Carpinteri and Spagnoli [20, 21]. The model introduced a new parameter, k_n, called normal stress sensitivity. All these models are based on the directional cosines of the vector normal to the critical plane (l,m,n). The damage ratio is calculated directly, but not the fatigue life.

The damage model of McDiarmid [18, 19] is expressed as

$$\frac{\tau_a(l_M, m_M, n_M)}{\tau_{f_{-1}}} + \frac{\sigma_{n,max}(l_M, m_M, n_M)}{2S_u} = D \tag{2.18}$$

where τ_a is shear stress amplitude, $\sigma_{n,max}$ is maximum normal stress and $\tau_{f_{-1}}$ is shear fatigue limit for fully reversed torsion.

The damage model of Carpinteri and Spagnoli [20, 21] is expressed as

$$\left[\left(\frac{\tau_a(l_C, m_C, n_C)}{\tau_{f_{-1}}}\right)^2 + \left(\frac{\sigma_{n,max}(l_C, m_C, n_C)}{\sigma_{f_u}}\right)^2\right]^{1/2} = D \tag{2.19}$$

where σ_{f_u} is uniaxial fatigue limit.

The fatigue model proposed by Ninic [17] gives the damage parameter as

$$\left[\left(\frac{\tau_a(l_D, m_D, n_D)}{\tau_{f_{-1}}}\right)^2 + k_n\left(\frac{\sigma_{n,max}(l_D, m_D, n_D)}{\sigma_{f_u}}\right)^2\right]^{1/2} = D \tag{2.20}$$

where k_n is normal stress sensitivity factor. Its formulation for uniaxial loading is given by

$$k_n = \left(\frac{\sigma_{f_u}}{\tau_{f_{-1}}}\right)^2 \left[1 - \left(\frac{\sigma_{f_u}}{2\tau_{f_{-1}}}\right)^2\right] \tag{2.21}$$

The developed model was validated empirically for mild steel, hard steel, cast iron and aluminum 6082-T6, and k_n was found with solid bar specimens.

Ninic and Stark [22] extended the study in [17]. The model was compared with ellipse quadrant and ellipse arc models [23] in addition models in [18-21]. Also, the models were compared for various loading conditions i.e. proportional, non-proportional, in-phase and out-of-phase cases.

The damage parameters of ellipse quadrant and ellipse arc models were respectively given as

$$\left[\left(\frac{\tau_a}{\tau_{f_{-1}}}\right)^2+\left(\frac{\sigma_a}{\sigma_{f_u}}\right)^2\right]^{1/2}=D \tag{2.22}$$

$$\left[\left(\frac{\tau_a}{\tau_{f_{-1}}}\right)^2+\left(\frac{\sigma_a}{\sigma_{f_u}}\right)^2\left(\frac{\sigma_{f_u}}{\tau_{f_{-1}}}-1\right)+\left(\frac{\sigma_a}{\sigma_{f_u}}\right)\left(2-\frac{\sigma_{f_u}}{\tau_{f_{-1}}}\right)\right]^{1/2}=D \tag{2.23}$$

where σ_a is axial stress amplitude.

There are numerous damage models in the literature. Some of them relates the damage parameter to fatigue life of material with using geometry and loading parameters where some concentrates to develop a methodology for finding the damage parameter.

In order to develop a multiaxial high cycle fatigue damage model with stress-based approach Liu and Mahadevan [24] introduced a new characteristic plane criterion, which is quite different from the previous definitions of critical plane. Like the critical plane approach, the model first identifies the critical plane and stress components on this plane, but it uses the dimension reduction of the deformed material. The formulation of the model involves a the combination of axial and shear stress amplitudes as well as hydrostatic stress amplitude with some model parameters. This is simply

$$\sqrt{(\frac{\sigma_{a,\alpha}}{\sigma_{f_{-1}}})^2+(\frac{\tau_{a,\alpha}}{\tau_{f_{-1}}})^2+k_l(\frac{\sigma_{a,\alpha}^H}{\sigma_{f_{-1}}})^2}=\beta_l \tag{2.24}$$

where $\sigma_{a,\alpha}$, $\tau_{a,\alpha}$, and σ_a^H are axial, shear and hydrostatic stress amplitude acting on the characteristic plane where α indicates the angle between the characteristic plane and maximum normal stress plane, k_l and β_l are material parameters. In order to find k_l, β_l and α, the characteristic plane must be defined. It may be the maximum normal or maximum shear stress plane. In order to choose between them, a new parameter, s, is introduced and it is simply defined as the ratio of fatigue limits of torsional and uniaxial loads, $s=$

$\tau_{f_{-1}}/\sigma_{f_{-1}}$. They [24] presented a table for these material and plane parameters for values of s larger than 1.0 and also for values less than 1.0. Since, these parameters are formulated only with a single variable s, it is quite clear to find them once the fatigue limits of the material are known in tension and torsion.

Additionally, the formulation is extended with the addition of mean normal stress component. However, the mean shear stress effect is skipped for this model. After modification, the formulation becomes

$$\frac{1}{(1-\frac{\sigma_{m,max}}{\sigma_{ref}})}\sqrt{(\frac{\sigma_{a,\alpha}}{\sigma_{f_{-1}}})^2+(\frac{\tau_{a,\alpha}}{\tau_{f_{-1}}})^2+k_l(\frac{\sigma^H_{a,\alpha}}{\sigma_{f_{-1}}})^2}=\beta_l \tag{2.25}$$

where $\sigma_{m,max}$ is mean normal stress on maximum normal plane and σ_{ref} is the reference stress which can be calibrated with uniaxial test. However, authors indicated that taking the reference stress as ultimate tensile strength gave very accurate results; thus, performing experimental tests with mean stress were not needed.

Based on these formulations, fatigue life model was presented as

$$\frac{1}{\beta_l}\frac{1}{(1-\frac{\sigma_{m,max}}{\sigma_{ref}})}\sqrt{(\sigma_{a,\alpha})^2+\left(\frac{\sigma'_f}{\tau'_f}\right)^2(\tau_{a,\alpha})^2+k_l(\sigma^H_{a,\alpha})^2}=\sigma'_f \tag{2.26}$$

Another critical plane approach was developed by Rashed *et al.* [5]. The model predicts crack initiation life based on the loading conditions and available biaxial material data; in this respect it is suitable for shape optimization since it does not have a geometric parameter. The model gives two formulations for both shear cracking mode and normal cracking mode. Using Ramberg-Osgood's and stress concentration factor equations, the model is adopted to Socie [25] for multiaxial fatigue loading. These are stated below for shear and normal cracking modes, respectively as

$$\gamma_{a,max}\left(1+k\frac{\sigma_{n,max}}{\sigma_y}\right)=\frac{\tau_f'}{G}(2N_f)^{b'}+\gamma_f'(2N_f)^{c'} \quad \text{for shear cracking mode} \tag{2.27}$$

$$\sigma_{max}\varepsilon=\frac{\sigma_f'^{\,2}}{E}(2N_f)^{2b}+\sigma_f'\varepsilon_f'(2N_f)^{b+c} \quad \text{for axial cracking mode} \tag{2.28}$$

where $\gamma_{a,max}$ is the maximum shear strain amplitude and k_r is a material parameter.

The parameters $\gamma_{a,max}$, $\sigma_{n,max}$, σ_{max} and ε are determined from local stress and strain response at a notch. All other material constants are obtained from smooth specimen fatigue data. Additionally, the authors verified the model by conducting experiments on SAE 1045 steel. Substituting the material constants for of this material, the above equations become

$$\gamma_{a,max}=0.0059N_f^{-0.09}+0.30N_f^{-0.44} \quad \text{for shear cracking mode} \tag{2.29}$$

$$\sigma_{max}\varepsilon=3.9N_f^{-0.18}+169.9N_f^{-0.54} \quad \text{for axial cracking mode} \tag{2.30}$$

Since the model gives two separate equations for shear and normal cracking mode, one should know which cracking mode is more critical for a particular application.

Fatemi and Yang [26] gives a review of fatigue damage theories and models including, linear damage rules, damage curve approaches, crack growth theories and energy based damage theories. The followings are the characteristics of these models:

$$D=\sum D_i=\sum {N_i}\Big/{N_{fi}} \quad \text{linear damage rule [27]} \tag{2.31}$$

where D_i is cycle ratio and N_i/N_{f_i} are applied life ratio for the ith load level.

Miller [28] presented two crack growth models for microstructurally short crack (MSC) and physically small crack (PSC).

$$\frac{da}{dN} = A^{msc}(\Delta\gamma)^{\alpha_m}(d-a) \quad \text{for MSC} \tag{2.32}$$

$$\frac{da}{dN} = B^{psc}(\Delta\gamma)^{\beta_m}a - C_g \quad \text{for PSC} \tag{2.33}$$

where α is crack length, A^{msc}, B^{psc}, α_m and β_m are material constants obtained from curve fitting of experimental data, d is barrier size, C_g is crack growth rate and $\Delta\gamma$ is shear strain range.

Finally, the following equation shows Leis's [29] energy-based nonlinear fatigue model;

$$D = \frac{4\sigma_f'}{E}(2N_f)^{2b_1} + 4\sigma_f'\varepsilon_f'(2N_f)^{b_1+c_1} \tag{2.34}$$

where b_1 and c_1 are different from fatigue strength and ductility exponents. They are related to the instantaneous strain-hardening exponent.

2.2. Energy Models

Łagoda [30] presented a model that related strain energy density parameter to the fatigue strength and life of materials. Although the model was proposed for uniaxial and random loading, it has potential to be applicable for multiaxial case. The formulation is based on Coffin-Manson-Basquin general fatigue model equation given by

$$\varepsilon_a = \varepsilon_a^e + \varepsilon_a^p = \frac{\sigma_f'}{E}(2N_f)^b + \varepsilon_f'(2N_f)^c \tag{2.35}$$

where ε_a^e, ε_a^p and ε_a are elastic, plastic and total strain amplitudes. Then Łagoda [30] makes use of previously proposed strain energy density models, which are

$$logU_f = A_m' - b_m' \log N_f \quad \text{Mrozinki's Model [31]} \tag{2.36}$$

$$U_f = A_k(N_f)^{v_k} \quad \text{Kaleta's Model [32]} \tag{2.37}$$

where U_f is the total strain energy density and the remaining terms are model parameters that depend on material and geometry. Łagoda [30] modified these equations to obtain

$$U_t = \frac{2(1+\nu){\sigma_f'}^2}{3E}(2N_f)^{2b} + 4\sigma_f'\varepsilon_f'(\frac{c-b}{c+b})(2N_f)^{b+c} \tag{2.38}$$

where U_t is the strain energy density in a fatigue cycle corresponding to peak stress and it should be noted that U_t includes all components of strain energy. After modification of Coffin-Manson-Basquin energy model, Equation 2.35, to, fatigue life is related to strain energy as

$$U_a = \frac{\left(\sigma_f'\right)^2}{2E}(2N_f)^{2b} + 0.5\varepsilon_f'\sigma_f'(2N_f)^{b+c} \tag{2.39}$$

where U_a is the alternating strain energy density. The elastic tem dominates in HCF, then

$$U_a = \frac{\left(\sigma_f'\right)^2}{2E}(2N_f)^{2b} \tag{2.40}$$

After taking the logarithm of both sides in Equation 3.4, one obtains

$$logN_f = A' - m'logU_a \tag{2.41}$$

where $A' = -\frac{1}{2b}[log\frac{\left(\sigma_f'\right)^2}{2E} + 2blog2]$ and $m' = 1/2b$. After all, fatigue limits in energy form can be written as

$$U_f = \frac{\sigma_f^2}{2E} \tag{2.42}$$

where subscript "f" denotes fatigue limit.

Łagoda [33] then investigated the validity of the model by comparing the model prediction with experimental results for various steels. These were 10HNAP, two forms of 18G2A, GGG40, GGG60, 35NCD16 and 12010.3. The static, cyclic and Wöhler's parameters (m' and U_{af}) for these materials were provided. Additionally, comparisons were not only made with the empirical data, but also with the results of other models, and the most accurate model for each material was noted.

Jahed and Farahani [34] provided two formulations for fatigue life; one is for axial loading and the other for torsional loading. The model uses Basquin-Coffin-Manson relations for pure axial and pure torsional cases as in Equations 2.14 and 2.15 to obtain energy based fatigue lifetime equations as

$$\Delta E_A = E'_e(N_A)^B + E'_f(N_A)^C \tag{2.43}$$

$$\Delta E_T = W'_e(N_T)^{B_s} + W'_f(N_T)^{C_s} \tag{2.44}$$

where ΔE_A and ΔE_T are the energies due to purely tensile and purely torsional loadings, E'_e and W'_e are axial and shear fatigue strength coefficients in energy base, E'_f and W'_f are axial and shear fatigue ductility coefficients in energy base, B and B_s are axial and shear fatigue strength exponents in energy base, C and C_s are axial and shear fatigue ductility exponents in energy base, and N_A and N_T are axial and torsional fatigue lives, respectively. The resulting fatigue life for multiaxial loading can be obtained by

$$N_f = \frac{\Delta E_A}{\Delta E} N_A + \frac{\Delta E_T}{\Delta E} N_T \tag{2.45}$$

where ΔE is the total energy obtained from cyclic hysteresis loop. The model was experimentally verified with tests on SAE 1045, AISI 304 and Inconel 718 materials. The model predicts the fatigue lifetime with a factor of ±1.8, ±1.2 and ±1.3 for SAE 1045, Inconel 718 and AISI 304 (SS304), respectively.

The relation between energy dissipation and fatigue life was studied by Ozaltun *et al.* [35]. The fatigue life was defined as the ratio of the total monotonic energy density to strain energy density for one cycle. This is expressed as

$$N = C^{O}\frac{\sigma_{ne}\left(\varepsilon_{ne}-\frac{\sigma_{ne}}{2E}\right)+\varepsilon_0\sigma_0\left[\cosh\left(\frac{\sigma_{ne}}{\sigma_0}\right)-1\right]+\frac{\beta_1^O}{2}\left(\varepsilon_f^2-\varepsilon_{ne}^2\right)+\beta_0^O\left(\varepsilon_f-\varepsilon_{ne}\right)}{2\sigma_c\left\{\frac{\sigma_a}{\sigma_c}\sinh(\frac{2\sigma_a}{\sigma_c}-\left[\cosh\left(\frac{2\sigma_a}{\sigma_c}\right)-1\right]\right\}} \quad (2.46)$$

where σ_{ne} is the necking stress, ε_f is fracture strain, ε_{ne} is the necking strain, β_0^O, β_1^O, ε_0 and σ_0 are curve fit parameters obtained from monotonic stress-strain curve, σ_c and C^O are curve fit parameters obtained from cyclic stress-strain hysteresis loop. The material tested was Al6061-T6, and the experiments were done with $R=-1$, fully reversed loading. Additionally, plastic strain energy dissipated per cycle until threshold is given as

$$U_f^p = \frac{2\sigma_c}{C^O}\left\{\frac{\sigma_a}{\sigma_c}\sinh\left(\frac{2\sigma_a}{\sigma_c}\right)-\left[\cosh\left(\frac{2\sigma_a}{\sigma_c}\right)-1\right]\right\} \quad (2.47)$$

where U_f^p is plastic strain energy dissipated per cycle. Also, Table 2.1 [35] below shows the plastic energy dissipated for various cycle ranges.

Table 2.1. Plastic strain energy dissipation for 0.05 Hz loading frequency [35].

Cycles	[-]	0-10 K	0-20 K	0-30 K	0-40 K	0-50 K	0-54 K	0-56 K
Energy	[MJ/m^3]	7.1	14.3	21.1	29.0	32.3	36.9	119.6

From, Table 2.1 it can be seen that 54 K is the threshold cycles. From experiments, authors [35] state that threshold point requires 10% of material toughness computed from monotonic tension test. Therefore, for the stated material, threshold fatigue life is given in Equation 2.48.

Although the study gives a direct calculation between monotonic tensile properties and fatigue life, the paper contains only axial fatigue test and calculation for fully reversed

loadings. It is somehow questionable whether the model can be adopted for multiaxial cases. The parameter is given for aluminum that was tested in that study, but it is quite easy to find these values for steels from literature since they are basic monotonic and fatigue parameters. Although there is no statement about the applicability of the model to multiaxial cases, it may be used by using equivalent stress and strain components.

$$N = C^{O}\frac{0.1\left\{\sigma_{ne}\left(\varepsilon_{ne}-\frac{\sigma_{ne}}{2E}\right)+\varepsilon_0\sigma_0\left[\cosh\left(\frac{\sigma_{ne}}{\sigma_0}\right)-1\right]+\frac{\beta_1^O}{2}\left(\varepsilon_f^2-\varepsilon_{ne}^2\right)+\beta_0^O\left(\varepsilon_f-\varepsilon_{ne}\right)\right\}}{2\sigma_c\left\{\frac{\sigma_a}{\sigma_c}\sinh(\frac{2\sigma_a}{\sigma_c}-[\cosh\left(\frac{2\sigma_a}{\sigma_c}\right)-1]\right\}} \tag{2.48}$$

Gasiak and Pawliczek [36] represented a direct calculation of fatigue life of materials by using the mean stress and strain values with some model parameters that are determined experimentally. They expressed mean strain, ε_m in terms of mean stress, σ_m and function of asymmetry sensitivity, $\Psi(N_f)$, as

$$\varepsilon_m = \frac{\Psi(N_f)}{E}\sigma_m \tag{2.49}$$

The relation between this function and fatigue life is expressed as

$$\Psi\left(N_f\right) = \eta_g N_f^{\lambda_g} \tag{2.50}$$

where η_g and λ_g are material and loading parameters, which were found for 18G2A and 10HNAP steels by the authors given in Table 2.2 [36].

Table 2.2. Mathematical form of asymmetry function parameters for 18G2A and 10HNAP [36].

Steel	Bending	Torsion	Bending with torsion
18G2A	$\Psi(N_f) = 3.124N_f^{-0.162}$	$\Psi(N_f) = 2.890N_f^{-0.148}$	$\Psi(N_f) = 0.854N_f^{-0.044}$
10HNAP	$\Psi(N_f) = 1.006N_f^{-0.072}$	$\Psi(N_f) = 0.818N_f^{-0.113}$	$\Psi(N_f) = 0.066N_f^{-0.113}$

The experimental study shows that most of results fall into 1/3 prediction scale with the predictive model results for bending, torsion and bending with torsion cases. The study seems very applicable to optimization study in finite element analysis (FEA), since a direct calculation seems to be given between fatigue life and model and material parameters that were presented by authors. However, the accuracy of the model for notched components seems questionable.

2.3. Crack and Fracture Mechanics Based Models

Peeker and Niemi [37] used crack initiation and stable growth phenomena in order to predict fatigue life with the relation of crack length. Starting with crack behavior of materials, authors investigated the crack propagation in two parts. These are fatigue threshold regime and stable growth regime. The former one is resulted from the elastic behavior of loading, and the latter one is resulted from plastic behaviors. The crack-life regimes were formulated for those separately as follows

$$\frac{da}{dN_f} = C_{el}\Delta K_c{}^{m_{el}} \tag{2.51}$$

where ΔK_c is stress concentration factor. C_{el} and m_{el} are defined as

$$C_{el} = 2\delta[(\sigma_f' - \sigma_m)\sqrt{2\pi\delta}]^{\frac{1}{b'}} \tag{2.52}$$

$$m_{el} = -\frac{1}{b'} \tag{2.53}$$

where δ is element size near crack. For the stable growth regime, equation of plastic components is stated as

$$\frac{da}{dN_f} = C_{pl}\Delta K_c{}^{m_{pl}} \tag{2.54}$$

Plastic crack parameters C_{pl} and m_{pl} are defined as

$$C_{pl} = 2\delta[\varepsilon_f' \left(\frac{4\pi\delta K' E}{n+1}\right)^{\frac{1}{n+1}}]^{\frac{1}{c'}} \tag{2.55}$$

$$m_{pl} = -\frac{1}{c'(n+1)} \tag{2.56}$$

where K' is cyclic strength coefficient.

Finally, the stress concentration factor at the intersection of these two regimes is calculated as

$$\Delta K_c^* = (\frac{C_{el}}{C_{pl}})^{\frac{1}{m_{pl}-m_{el}}} \tag{2.57}$$

There is nearly no applicability of this model [37] to our study, since the crack regime and crack length approach is not suitable for optimization problems. We should concentrate on more general and direct forms where some crack models to fatigue problems will also be studied.

Another study by Panasyuk and Sylovanyuk [38] presents a model for predicted fatigue life with considering the crack initiation and propagations. Formulation of the fatigue life until crack initiation may be helpful for our study which is

$$N_f = [\frac{(\varepsilon_u - \varepsilon_e)^m}{\Delta\varepsilon_{-e}{}^m}(1-mk)+1]^{1/(1-mk)} \tag{2.58}$$

where ε_u is ultimate level of strain, m and k are material crack parameters, and $\Delta\varepsilon_{-e}$ is inelastic strain range. Defining the plastic or elastic part of the strain in FEA is the problem, since it gives total or equivalent strains.

Yuen and Taheri [39] presented a modification to the Zheng and Hirt [40] fatigue model. Zheng and Hirt model is

$$\frac{da}{dN_f} = B^{zh}\Delta K_{eff}^2 = \frac{1}{2\pi\sigma_{ff}^2}(\Delta K - \Delta K_{th})^2 \tag{2.59}$$

where B^{zh} is Zheng and Hirt [40] parameter, ΔK is stress intensity factor, ΔK_{eff} applied effective stress intensity factor, ΔK_{th} is fatigue crack growth threshold and σ_{ff} is critical fracture stress. Authors [40] calculated B^{zh} parameter with considering the ultimate tensile strength as the maximum nominal stress. However, Yuen and Taheri [39] opposed to this and run tension test to obtain true stress at fracture. Authors [39] represented B^{zh} parameters for various materials those were predicted by Zheng and Hirt and reanalyzed them with their true stress criteria at fracture time. Finally, Yuen and Taheri [39] showed that model in [40] overpredicts B^{zh} values for most of the cases.

For experimental study, authors [39] selected 350WT steel and found the model equation for both Zheng and Hirt model, and modification of it.

$$\frac{da}{dN_f} = 6.47x10^{-10}(\Delta K - 5.76)^2 \quad \text{Zheng and Hirt Model [40]} \tag{2.60}$$

$$\frac{da}{dN_f} = 4.17x10^{-10}(\Delta K - 8.64)^2 \quad \text{Model in [39]} \tag{2.61}$$

There are various fatigue models in the literature in addition to ones that were examined in Sections 2.1, 2.2 and 2.3. Models proposed in [6, 7, 41-49] all have a common point that they used axial and/or torsional fatigue limits to calculate fatigue life or damage parameter. Since the fatigue limit parameters are highly affected by geometry of the material, they cannot be applicable to shape optimization process. At this point, it is now more obvious that the model which does not use parameters related to geometry, such as fatigue limit, would be very useful to shape optimization problems.

3. PROPOSED MODEL

In this study, an energy approach is adopted. Considering that in HCF, the effects of plastic deformations on fatigue life are negligible [30, 33], fatigue life of a material in the HCF range mostly depends on elastic cyclic hysteresis and plastic terms can be omitted. This means that crack initiation is the dominant phase for HCF conditions [2, 17, 22, 47, 50]. Crack propagation has less importance and significant portion of the fatigue life passes during initiation of microcracks.

The proposed model is based on the alternating elastic strain energy density U_a which is expressed in terms of alternating elastic stress, σ_a, and strain ε_a, as

$$U_a = \int_{\varepsilon_1}^{\varepsilon_2} \sigma_a d\varepsilon_a = \frac{\sigma_a \varepsilon_a}{2} = \frac{E\varepsilon_a^2}{2} \tag{3.1}$$

Coffin-Manson-Basquin relation [1] states that

$$\varepsilon_a = \frac{\sigma_f'}{E}(2N_f)^b + \epsilon_f'(2N_f)^c \tag{3.2}$$

where σ_f' is the axial fatigue strength coefficient, ε_f' is the axial fatigue ductility coefficient, b is the axial fatigue strength exponent, c is the axial fatigue ductility exponent, E is the elastic modulus and N_f is the number of cycles to failure. Since the second term accounts for the effect of plastic deformation, in HCF the equation simplifies to

$$\varepsilon_a = \frac{\sigma_f'}{E}(2N_f)^b \tag{3.3}$$

Substituting Equation 3.3, Equation 3.1 becomes

$$U_a = \frac{\left(\sigma_f'\right)^2}{2E}(2N_f)^{2b} \tag{3.4}$$

Equation 3.4 is valid only if axial strain is dominant on the fatigue life of the material [51]. For the shear strain dominant fatigue behavior, the relation can be written as

$$U_a = \frac{\left(\tau_f'\right)^2}{2G}\left(2N_f\right)^{2b'} \tag{3.5}$$

where τ_f' is the shear fatigue strength coefficient, b' the is shear fatigue strength exponent and G the is shear modulus.

Equation 3.4 and 3.5 will be called as axial dominant and shear dominant fatigue models, respectively.

3.1. Introducing Equivalent Strain Energy Density

The relation between strain energy density and fatigue life in Equations 3.4 and 3.5 is valid for uniform parts under uniaxial loading, but not for parts containing a notch or an irregular shape leading to stress concentration. Knowing that fatigue cracks in HCF always initiate from a micro crack or a micro flaw, crack initiation depends on the number of micro flaws, and therefore on the size of the stressed region. For this reason, calculating the strain energy density based on the maximum stress or strain yields overly conservative predictions; there may not be a micro flaw at the point where the maximum stress develops. On the other hand, calculation based on the arithmetic average of strain values will result in highly nonconservative predictions. Because of the sensitivity of crack initiation on stress level, highly stressed regions will be much more effective on fatigue life than low stressed regions.

In this study, an approach based on equivalent strain energy is proposed to account for the effect of a notch, or a stress concentration on fatigue life. Equivalent strain energy parameter should correctly reflect the effects of the severity of stress concentration and the size of the highly stressed region, and also it should be defined in general terms without being specific to particular notch geometry.

Because analytical solution is available only for a limited number of part geometries, finite element modeling (FEM) is generally used to determine the stress and strain states in the parts. Once, FEA is carried out and the stress and strain components, σ_{ij}^{k} and ε_{ij}^{k}, in element k, are determined corresponding to minimum and maximum loads, their alternating values, $\sigma_{aij}^{k} = (\sigma_{ij.max}^{k} - \sigma_{ij.mln}^{k})/2$ and $\varepsilon_{aij}^{k} = (\varepsilon_{ij.max}^{k} - \varepsilon_{ij.mln}^{k})/2$ are calculated. The alternating strain energy density, U_a^k, in that element can be calculated using the following formula:

$$U_a^k = \frac{1}{2}\sum_{i=1}^{3}\sum_{j=1}^{3}\sigma_{ij}^{k}\varepsilon_{ij}^{k} \tag{3.6}$$

The life of material in element k, N_f^k, is calculated using Equations 3.4 and 3.6:

$$U_a^k = \frac{\left(\sigma_f'\right)^2}{2E}(2N_f^k)^{2b} \tag{3.7}$$

Endurance limits of steels correspond to about 10^6 load cycles [52]. This means that if the calculated fatigue life is higher than this value, it is assumed to have infinite life. Accordingly, the finite elements having fatigue life longer than 10^6 according to Equation 3.7 are assumed not to contribute to the fatigue life of the member itself. In the fatigue assessment procedure developed in this study, the threshold strain energy density, U_a^{th}, which corresponds to 10^6 cycles, can be calculated by

$$U_a^{th} = \frac{(\sigma_f')^2}{2E}(2.10^6)^{2b} \tag{3.8}$$

Then, only the elements having strain energy amplitudes greater than U_a^{th} are considered. Based on the strain energies of these elements equivalent strain energy is defined. If the arithmetic mean were taken as equivalent value, which is

$$U_{avg} = \frac{1}{n}\sum_{k=1}^{n}U_a^k \tag{3.9}$$

where n is the number of elements that have fatigue life lower than 10^6, the fatigue life of the specimen would be highly underestimated, because highly stressed regions will actually have more determining effect than the low stressed regions. Typically a 10% increase in stress level may reduce the life to its half. U_a^k in Equation 3.9 should be multiplied by a factor that includes this effect. The fatigue model presented in Equations 3.4 and 3.5 already reflects this effect; in other words $(2N_f)^{2b}$ and $(2N_f)^{2b'}$ already accounts for this effect. Accordingly, these terms are used as a factor, in the definition of equivalent strain energy density, then the equation is normalized by their sum as follows

$$U_{ea} = \frac{\sum_{k=1}^{n}(2N_f^k)^{2b}U_a^k}{\sum_{k=1}^{n}(2N_f^k)^{2b}} \tag{3.10}$$

where $2N_f^k$ and U_a^k are the number of reversals to failure and the alternating strain energy density in element k, respectively.

Element sizes in a typical finite element mesh are nonuniform. The above formulation, however, does not account for different contributions of elements due to differences in size. In order to take into account the effect of the element size, a volume bias factor is included in the formulation as

$$U_{ea} = \frac{\sum_{k=1}^{n}V_k(2N_f^k)^{2b}U_a^k}{\sum_{k=1}^{n}V_k(2N_f^k)^{2b}} \tag{3.11}$$

where V_k is the volume of element k. After calculating U_{ea}, the fatigue life of the part, N_f, can be calculated by the following formulas:

$$U_{ea} = \frac{(\sigma_f')^2}{2E}(2N_f)^{2b} \quad \text{for axial dominant fatigue} \tag{3.12}$$

$$U_{ea} = \frac{(\tau_f')^2}{2G}(2N_f)^{2b'} \quad \text{for shear dominant fatigue} \tag{3.13}$$

4. NUMERICAL PROCEDURE

In this section, the procedure for the evaluation of the fatigue life and the finite element modeling are explained. Codes are developed using ANSYS Parametric Design Language (APDL) to implement the fatigue assessment model and carry out finite element analyses.

The procedure for finite element analysis has two main steps:

- Development of the FE model.
  - (i) Initialization of the program.
  - (ii) Pre-Processing.
    - Creating initial points.
    - Creating lines, areas and/or volumes.
    - Meshing the geometry.
    - Boundary conditions and solution.
- Post-Processing.

The first step, development of the FE model includes initialization of the program and pre-processing of the program. In the step called initialization of the program, the analysis type and initial parameters are defined. In the pre-processing step, material type and material properties (Young modulus and Poisson's ratio), key parameters (element size, absolute value of applied loads, yielding stress etc.) and output controls are defined. The model is developed. Key points are defined and lines that connect those points are created. After specified areas and/or volumes are formed, finite element mesh is generated. Lastly, force and displacement boundary conditions are defined and solution is obtained.

In the post-processing step, strain components in each element are obtained and the corresponding strain energy density values are calculated. The equivalent strain energy density expressed in Equations 3.12 and 3.13 is calculated using the programming capabilities of ANSYS.

Because the geometries, materials and loading conditions are different for each experimental study [53, 54], the FEA procedures also differ from each other. Therefore, they will be outlined separately.

4.1. FE Modeling and Fatigue Analysis of Specimen-1

First, comparisons are made between the results of the proposed fatigue model and experimental data [53] obtained on notched specimens in the shape of shouldered shaft made of SAE 1045 material. The specimen has a circular cross section with smooth fillets as depicted in Figure 4.1. The critical region is the fillet with a smaller radius of curvature. Because the specimen is axisymmetric, a 2D FE model is developed. The domain of analysis is shown in Figure 4.1 and Figure 4.2.

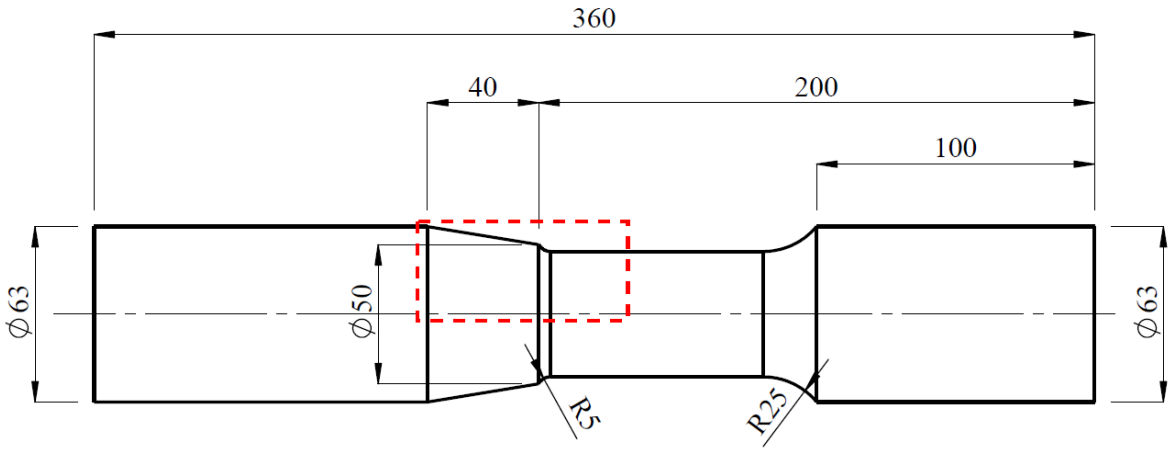

Figure 4.1. A scheme of the SAE 1045 notched specimen. The dimensions are in millimeters.

The pat of specimen-1 is subjected to fully reversed proportional loading with the cases of bending moment only, torsion only and combination of bending moment and torsion. The mechanical properties of SAE 1045 steel are given in Table 4.1.

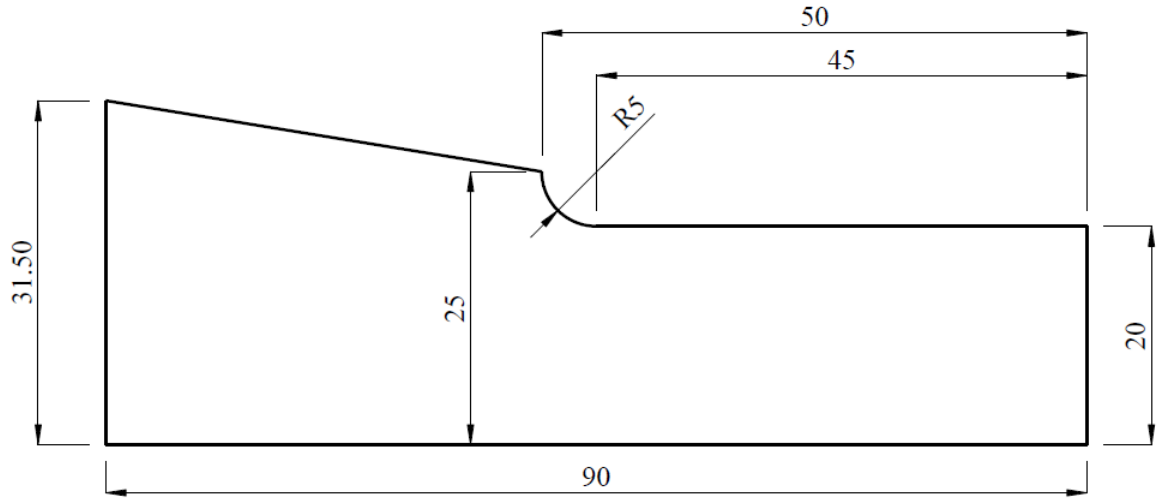

Figure 4.2. The part of the specimen analyzed by FEM. The dimensions are in millimeters.

Table 4.1. Mechanical properties of SAE 1045 steel [5, 53].

Young Modulus, E (GPa)	202
Poisson's Ratio, v	0.28
Shear Modulus, G (GPa)	79
Yield Stress, S_y (MPa)	200
Axial Fatigue Strength Coefficient, σ_f' (MPa)	948
Axial Fatigue Strength Exponent, b	-0.092
Shear Fatigue Strength Coefficient, τ_f' (MPa)	505
Shear Fatigue Strength Exponent, b'	-0.097

The APDL code for FEA is outlined in the following two sections.

4.1.1. Development of the FE Model for Specimen-1

This section of the APDL code includes the initial parameters and pre-processing part. Since the program is parametric, the user can change the values for the parameters and thus modify the model. These are mechanical specifications, analysis type, geometric parameters, load values and model specifications as element type.

In the finite element model of specimen-1, 2D elements with axisymmetric option is used. The name of the element type in ANSYS is PLANE83.

The notched is under uniform bending moment and/or torsion. Concentrated forces are applied to nodes as shown in Figure 4.3 that cause bending moment and torsion at the notch having magnitudes the same as the ones applied in the experiments. The concentrated forces applied in the z direction as shown in Figure 4.3 generates torsion. On the other hand, the forces applied in the x direction as force couples generates bending. In the region where point forces are applied, locally high stresses develop; but away from this region a smooth stress distribution corresponding to uniform torsion and bending prevails in accordance with Saint Venant's principle. In order to prevent this region from affecting the results, two measures are taken. First, the concentrated forces are distributed to a number of modes to reduce stress concentration. Secondly, the elements in the locally high stressed region are unselected during post-processing; in this way, they do not contribute to equivalent strain energy density.

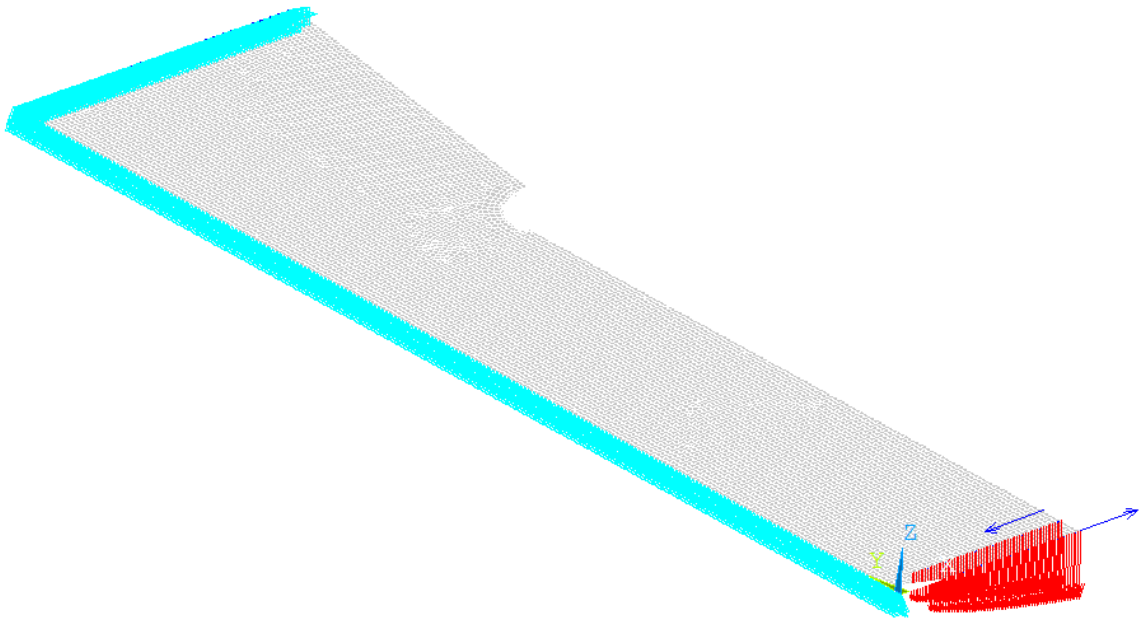

Figure 4.3. Boundary conditions of SAE 1045 notched shaft specimen.

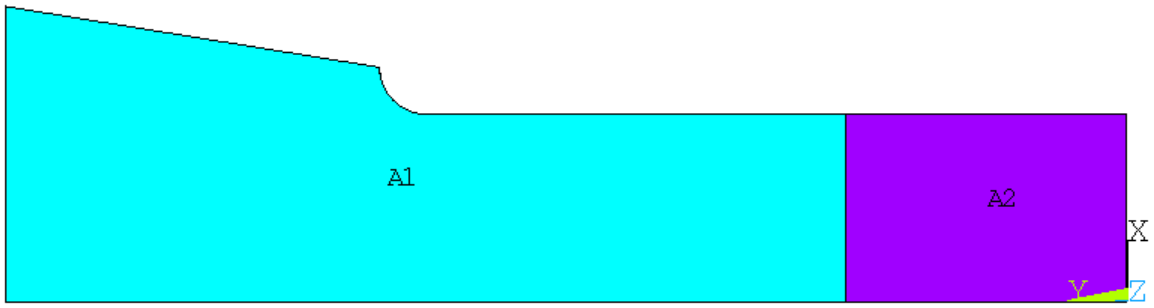

Figure 4.4. Schematic representation for material definition of SAE 1045 notched shaft specimen.

In Figure 4.4, A1 and A2 are the areas for the pre-defined two materials. In the post-processing section, the elements in the area A2 are unselected by using their material definition. The algorithm for material definition by specifying their mechanical properties (Young modulus and Poisson's ratio) is presented in Figure 4.5.

Define the first material;

```
MPTEMP,,,,,,,,
MPTEMP,1,0                  !defines the material type which is linear elastic isotropic
MPDATA,EX,1,,2.02E011       !defines Young modulus of material-1
MPDATA,NUXY,1,,0.28         !defines Poisson's ratio of material-1
```

Define the second material;

```
MPTEMP,,,,,,,,
MPTEMP,1,0                  !defines the material type which is linear elastic isotropic
MPDATA,EX,2,,2.02E011       !defines Young modulus of material-2
MPDATA,NUXY,2,,0.28         !defines Poisson's ratio of material-2
```

Figure 4.5. Material definition algorithm of APDL code for SAE 1045 notched shaft specimen.

In order to define the geometry, key points are defined and lines that connect these points are generated. After that, areas are created in the regions enclosed by those lines. The algorithm is explained in Figure 4.6.

Define initial points;

```
x1=0.025          !x coordinate of point-1
y1=0.080          !y coordinate of point-1
x2=0.0315         !x coordinate of point-2
y2=0.120          !y coordinate of point-2
```

Define lines;

```
l,1,2             !creates line between point-1 and point-2
larc,1,6,7,0.005  !creates arc line between point-1 and point-6, radius on the side of point-7 and with a value of 0.005
```

Define areas;

```
al,4,7,8,9        !creates area enclosed by point-4, point-7, point-8 and point-9
aglue,1,2         !combine area-1 and area-2
```

Figure 4.6. Geometry definition algorithm of APDL code for SAE 1045 notched shaft specimen.

After the areas are defined, a mesh is generated using 2D elements. For specimen-1, free mapped meshing operation is used with PLANE83 elements. Axisymmetric PLANE83 element is 8-node harmonic structural solid. The initial element size is defined as 0.5 mm. This restrains the each side of elements to be 0.5 mm or lower. However, in order to get sufficiently refined mesh, the arc line is refined around notch. The meshed geometry of specimen-1 is shown in Figure 4.7.

Once mesh geometry is generated, boundary conditions as forces and restraints are defined. Because the loading is multiaxial, different types of loads are applied in two separated steps. For bending load, *bending mode* command of ANSYS is used; and for

torsional load, *torsion mode* command is used. The results are separately obtained and superposed to obtain the resulting stress distribution.

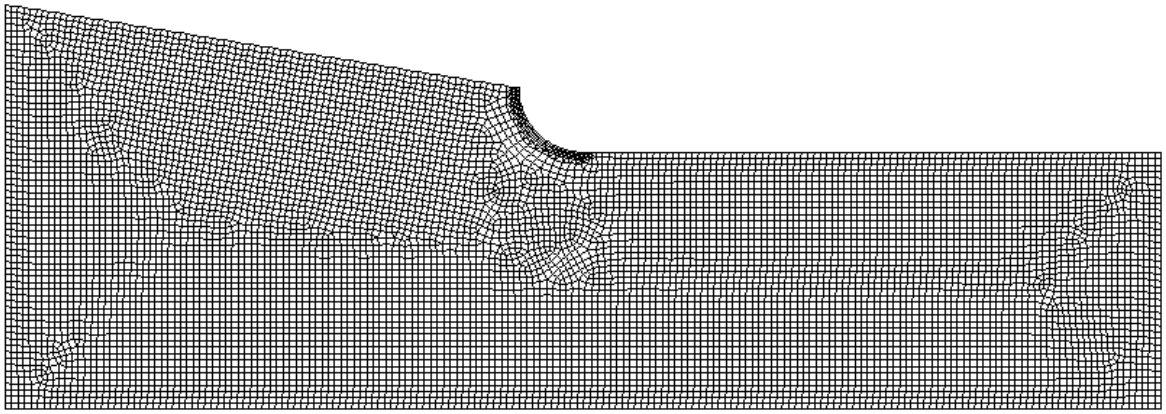

Figure 4.7. The meshed geometry of SAE 1045 notched shaft specimen.

The y axis in Figure 4.3 is defined as symmetry axis where nodes are fixed to zero displacement in the y direction and in the z direction, respectively for bending mode and torsion mode. Additionally, nodes on the left hand side are fixed in the y and z direction for both bending and torsion modes.

After defining the geometry, material properties, generating the mesh and defining the boundary conditions, *solve* command of APDL starts the analysis.

4.1.2. Post-Processing for Specimen-1

In the post-processing section, some analytical calculations are performed in order to transform the FEA results into more applicable variables that can be used to calculate fatigue life. The variable that is used for the proposed fatigue model is equivalent strain energy density that is described in Equations 3.12 and 3.13. In order to calculate U_{ea}, strain energy densities and areas of each element are stored by using *element table* command of APDL. The algorithms for the calculation of strain energy densities are represented in Figure 4.8.

define CriticalSENE *!strain energy density for $N_f = 10^6$ by using Equation 3.4 or Equation 3.5*
get TotElemNo *!Total element number in the model*
for k=1, k=TotElemNo
    if $U^k \geq$ CriticalSENE
        Calculate $(2N_f^k)^{2b}$ or $(2N_f^k)^{2b'}$ by using Equation 3.4 or Equation 3.5
        Get volume of each element
    end if
end for
for k=1, k=TotElemNo
    Calculate and **sum** $(2N_f^k)^{2b \; or \; 2b'} V^k$ of each element
end for
for k=1, k=TotElemNo
    Calculate U_{ea} by using Equation 3.12 or Equation 3.13 according to axial or shear dominant prediction
end for

Figure 4.8. Calculation algorithm of equivalent strain energy density.

ANSYS gives the equivalent strain energy density and other scalar parameters, which are defined by user in APDL code after the accompanying analysis. Since 2D axisymmetric analysis takes the geometry thickness as unity, volume of each element is same as the area of those.

The strain energy densities are stored in an array by using stress and strain components of each element. The general tensor form of the strain energy density is expressed in the following.

$$U = \frac{1}{2}\sum_{i=1}^{3}\sum_{j=1}^{3}\sigma_{ij}\varepsilon_{ij} \tag{4.1}$$

In the post-processing section of the APDL code, a simple addition to code can provide to visualize just the selected elements in that section, which are the ones having strain energy density higher than the threshold values, which is the one accompanying to 10^6 number of cycles to failure. It allows one to be sure that the selected elements are included in the specimen geometry where lengthening the geometry has no effect since no element can be added to calculation by this procedure.

4.2. FE Modeling and Fatigue Analysis of Specimen-2

The results of the model proposed in this study are also compared with the empirical data obtained in another experimental study performed by Jen and Wang [54]. The specimen has circular cross section with a circular hole in the center and it is made of AISI 316 material. The geometry of the specimen is drawn in Figure 4.9.

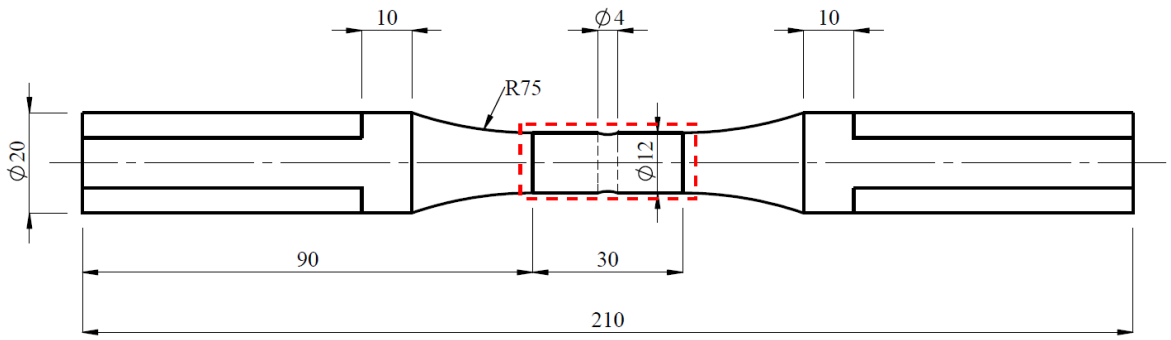

Figure 4.9. AISI 316 notched cylinder specimen. The dimensions are in millimeters.

As in specimen-1, the domain of analysis is not the whole specimen; but the critical region. As in the FE model in [54], the analyzed region is the narrowest part containing the hole as shown in Figure 4.10. The geometry is not axisymmetric as opposed to specimen-1. For this reason, 3D analysis is carried out.

The mechanical properties of the AISI 316 material are given in Table 4.2, where monotonic and axial fatigue properties are provided [54] and shear fatigue properties are provided in [55]. APDL code of specimen-2 is again outlined in two steps.

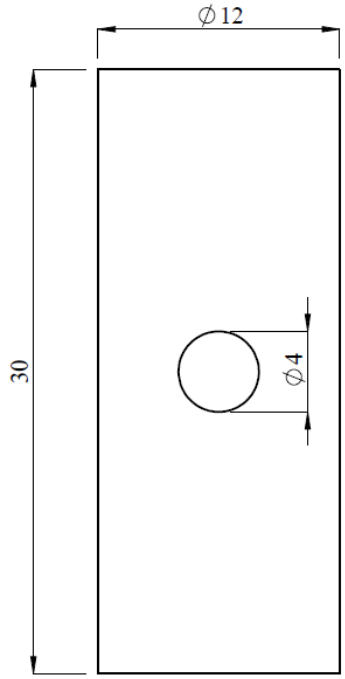

Figure 4.10. The analysis domain for AISI 316 notched cylindrical specimen. The dimensions are in millimeters.

Table 4.2. Mechanical properties of AISI 316 [54, 55].

Young Modulus, E (GPa)	192.68
Poisson's Ratio, v	0.3
Shear Modulus, G (GPa)	74.11
Yield Stress, S_y (MPa)	251.5
Axial Fatigue Strength Coefficient, σ_f' (MPa)	1,258.2
Axial Fatigue Strength Exponent, b	-0.097
Shear Fatigue Strength Coefficient, τ_f' (MPa)	385
Shear Fatigue Strength Exponent, b'	-0.050

4.2.1. Development of the FE Model for Specimen-2

For specimen-2, multiaxial loading is performed by applying concentrated forces on the nodes at the ends that induces axial and torsional loading in the notched region. The

resultant loads are given in terms of nominal stresses in [54] and their calculation will be explained in detail in Section 5.2. Since the point loads again create stress concentration around the their points of application, the domain of analysis is extended at both ends by 15 mm. Using the same procedure as the one for specimen-1, these additional parts are defined with another material with the same properties. Figure 4.11 shows the region of interest and the additional parts.

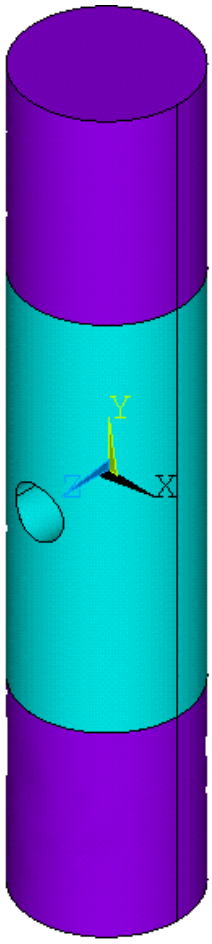

Figure 4.11. Schematic representation for material definition of AISI 316 notched cylinder specimen.

The additional volumes at the ends of Figure 4.11 are unselected by APDL code at the post-processing step and only the contribution of the inner region of the equivalent strain energy density is considered. The material definition algorithm (Young's modulus and Poisson's ratio) is the same as the one with specimen-1 stated in Figure 4.5.

In the pre-processing section of specimen-2, there is no need to define any initial key points and to create lines. Since the geometry of specimen-2 is cylindrical, the command *cylind* can create cylinders by specifying radius and height of the cylinder. The central hole is also created by first defining a cylinder with the same size and then subtracting form the main cylinder. The additional parts are also defined with *cylind* command and added to main cylinder to analyze and mesh. However, this command only creates cylinders that have cross section lying on the work plane. Since the work plane is x-y coordinate system in default, the working plane system should be rotated in order to create both hole geometry and main cylinders also with added parts. The geometry creation algorithm is defined as in Figure 4.12 in APDL code.

```
cylind,0.002,0,0.006,-0.006,0,360        !central hole cylinder with 0.002 m radius, 0.006m height in positive and negative z direction with 360° angle of rotation
wprota,0,90,0                            !rotation of working plane around y direction with 90°
cylind,0.006,0,0.015,-0.015,0,360        !main cylinder where the study focuses on
cylind,0.006,0,0.015,0.030,0,360         !added cylinder part on the top
cylind,0.006,0,-0.015,-0.030,0,360       !added cylinder part on the bottom
wpstyl,defa                              !setting the working plane to default orientation
vglue,2,3,4                              !added parts are glued to main cylinder
vsbv,2,1                                 !central hole is subtracted form cylinder
```

Figure 4.12. Geometry definition algorithm of APDL code for SAE 1045 notched shaft specimen.

After the definition of geometry, meshing operation takes place. The element type used for the 3D structural analysis is SOLID45 in ANSYS element library. SOLID45 is 3D tetrahedral structural element and defined with 8 nodes. Minimum element size is chosen as 1.25 mm and the elements on the surface around the central hole are refined with level of 4. The mesh geometry is shown in Figure 4.13.

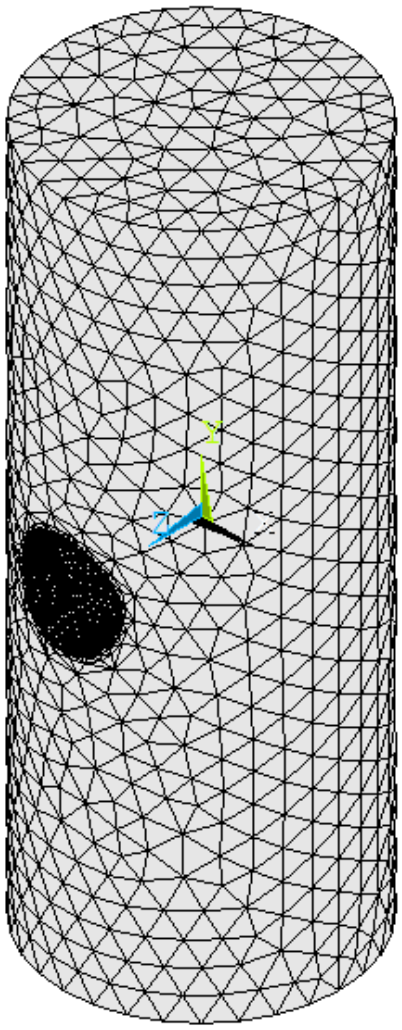

Figure 4.13. The meshed geometry of AISI 316 notched cylinder specimen.

After mesh generation, the forces are applied. Specimen is loaded with various axial and torsional loads. They are applied to top and bottom cross sections with same value since no symmetry condition can be applied in 3D model. Both axial and torsional loads are applied on four points of top and bottom cross sections in order to decrease the point wise stress concentration. This leads to division of the axial load by four. However, the

torsional loads are considered as force couples. Therefore, they are divided by two where two force couples are created on each cross section. Figure 4.14 shows the application of loads.

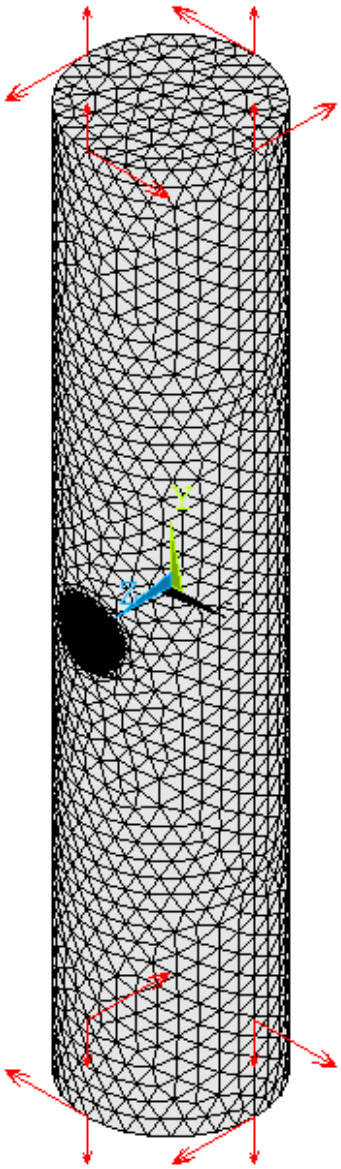

Figure 4.14. Boundary conditions of AISI 316 notched cylinder specimen.

4.2.2. Post-Processing for Specimen-2

The post-processing algorithm for specimen-2 is exactly same as the one for specimen-1, which is explained in Figure 4.8.

5. RESULTS & DISCUSSION

The model predictions are compared with the results of two experimental studies conducted on two different notched specimens made of two different materials, SAE 1045 and AISI 316. The details of the experimental setup are given in [53, 54]. Both of the specimens are subjected to multiaxial loadings which are combination of bending with torsional moment and axial load with torsional moment, respectively. The loading is fully reversed for both of them. Comparative results of specimen-1 and specimen-2 are outlined separately.

5.1. Comparative Results for Specimen-1

In Section 3.1, equivalent strain energy density approach is proposed for axial and shear dominant fatigue models. Comparisons are made for both of these models. Experiments were usually repeated a number of times for the same loading conditions. In comparisons, average of those experimental results are used.

A mesh convergence analysis is carried out to determine the number of elements necessary to accurately obtain the strain state. Table 5.1 presents equivalent strain energy densities, maximum strain energy densities and shear dominant fatigue life predictions for three different loading cases obtained with different element numbers. Besides, Figure 5.1, Figure 5.2 and Figure 5.3 show the mesh convergence results graphically. As the results indicate, totally 9,031 elements seem to be enough for mesh convergence where increasing the number of elements further has an effect on shear dominant fatigue life prediction no more than 1.08 %.

Table 5.2 gives the load levels applied in the experiments, number of cycles to failure until detection of initial crack and final fracture and the lives predicted using fatigue coefficient for axial and shear dominant modes. The loadings are listed in order or increasing fatigue life. Figure 5.4 graphically shows the comparison between model predictions and the experimental results provided by [53].

Table 5.1. Mesh convergence results of specimen-1.

Loading Case	Applied Bending Moment (N-m)	Applied Torsional Moment (N-m)	Number of Elements	Eqv. Strain Energy Density, U_{eqv} (Pa) (for shear)	Max. Strain Energy Density, U_{max} (Pa) (for shear)	Shear-Dominant Predicted Life, $N_{f(s)}$
2	2,800	0	400	3.28E+05	9.99E+05	1,836
2	2,800	0	445	3.26E+05	1.09E+06	1,895
2	2,800	0	655	3.31E+05	1.10E+06	1,762
2	2,800	0	1,091	3.34E+05	1.14E+06	1,691
2	2,800	0	3,095	3.34E+05	1.20E+06	1,669
2	2,800	0	3,355	3.34E+05	1.20E+06	1,671
2	2,800	0	4,594	3.36E+05	1.21E+06	1,639
2	2,800	0	5,798	3.36E+05	1.22E+06	1,640
2	2,800	0	7,573	3.36E+05	1.22E+06	1,641
2	2,800	0	9,031	3.35E+05	1.16E+06	1,643
2	2,800	0	15,756	3.36E+05	1.23E+06	1,634
2	2,800	0	26,824	3.36E+05	1.24E+06	1,636
11	1,850	2,100	400	2.70E+05	7.51E+05	5,057
11	1,850	2,100	445	2.67E+05	8.01E+05	5,298
11	1,850	2,100	655	2.73E+05	8.10E+05	4,714
11	1,850	2,100	1,091	2.78E+05	8.33E+05	4,331
11	1,850	2,100	3,095	2.77E+05	8.67E+05	4,380
11	1,850	2,100	3,355	2.76E+05	8.69E+05	4,472
11	1,850	2,100	4,594	2.78E+05	8.72E+05	4,343
11	1,850	2,100	5,798	2.77E+05	8.76E+05	4,381
11	1,850	2,100	7,573	2.78E+05	8.78E+05	4,313
11	1,850	2,100	9,031	2.78E+05	8.45E+05	4,359
11	1,850	2,100	15,756	2.78E+05	8.85E+05	4,351
11	1,850	2,100	26,824	2.78E+05	8.89E+05	4,330
8	0	3,000	400	2.48E+05	5.53E+05	7,821
8	0	3,000	445	2.58E+05	5.75E+05	6,371
8	0	3,000	655	2.59E+05	5.79E+05	6,295
8	0	3,000	1,091	2.56E+05	5.89E+05	6,618
8	0	3,000	3,095	2.57E+05	6.03E+05	6,509
8	0	3,000	3,355	2.57E+05	6.04E+05	6,475
8	0	3,000	4,594	2.57E+05	6.05E+05	6,448
8	0	3,000	5,798	2.57E+05	6.07E+05	6,467
8	0	3,000	7,573	2.58E+05	6.08E+05	6,409
8	0	3,000	9,031	2.57E+05	5.95E+05	6,503
8	0	3,000	15,756	2.57E+05	6.10E+05	6,475
8	0	3,000	26,824	2.57E+05	6.12E+05	6,433

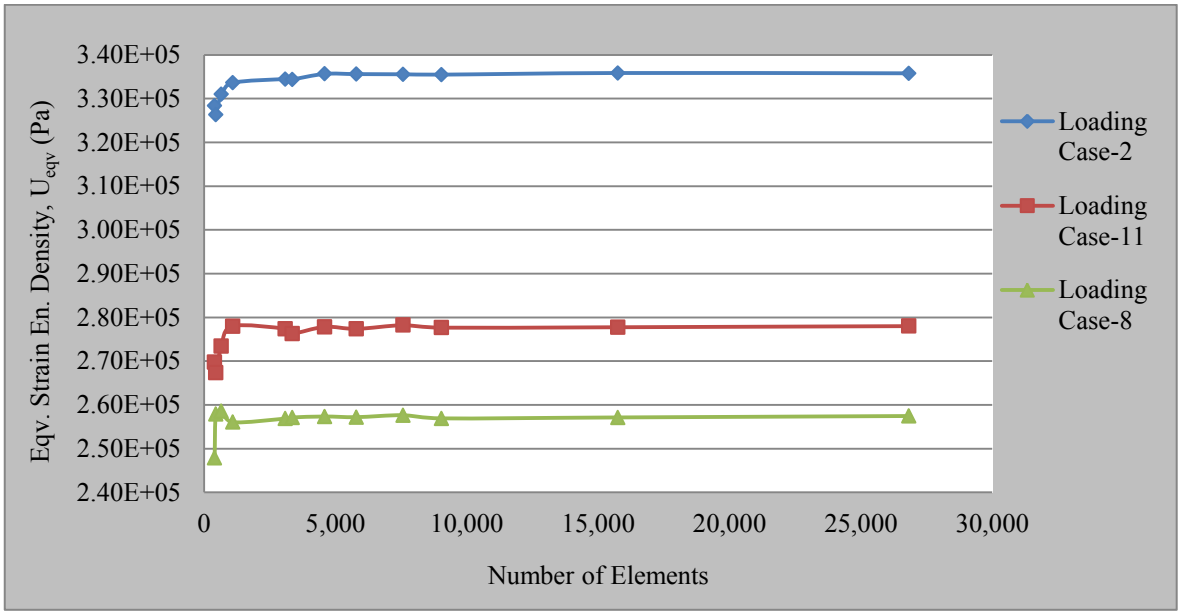

Figure 5.1. Mesh convergence for equivalent strain energy density, U_{eqv} of specimen-1.

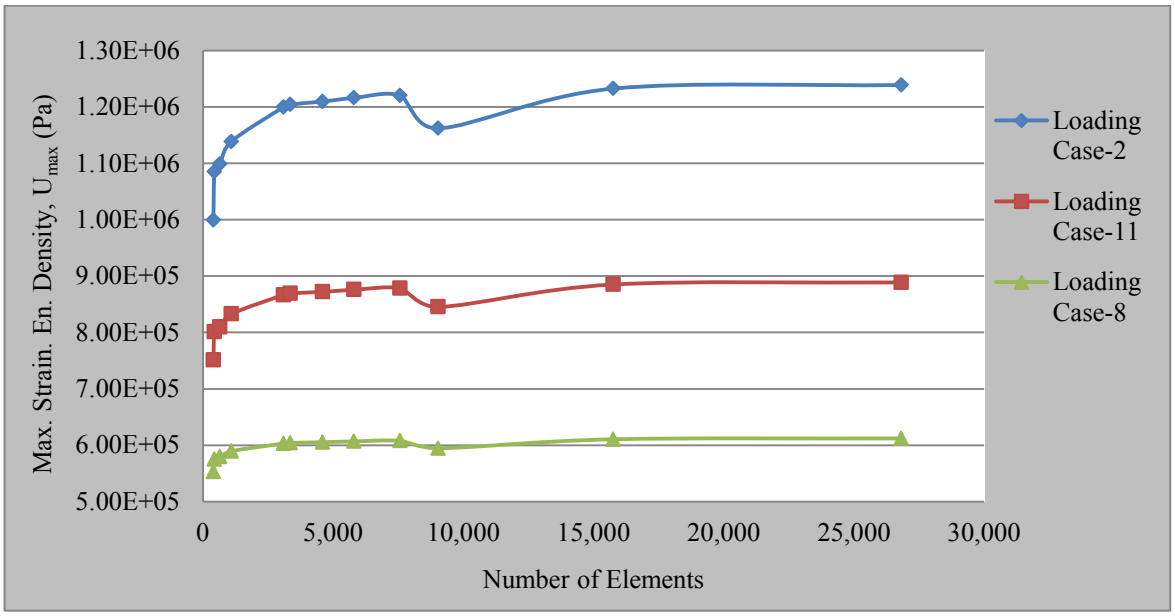

Figure 5.2. Mesh convergence for maximum strain energy density, U_{max} of specimen-1.

Considering that the model is developed to predict final failure, predictions of shear dominant fatigue model are sufficiently accurate. Except for only four cases, the trend of increasing fatigue life is correctly predicted where the ratio between measured life to predicted life lies between 0.96 and 5.0.

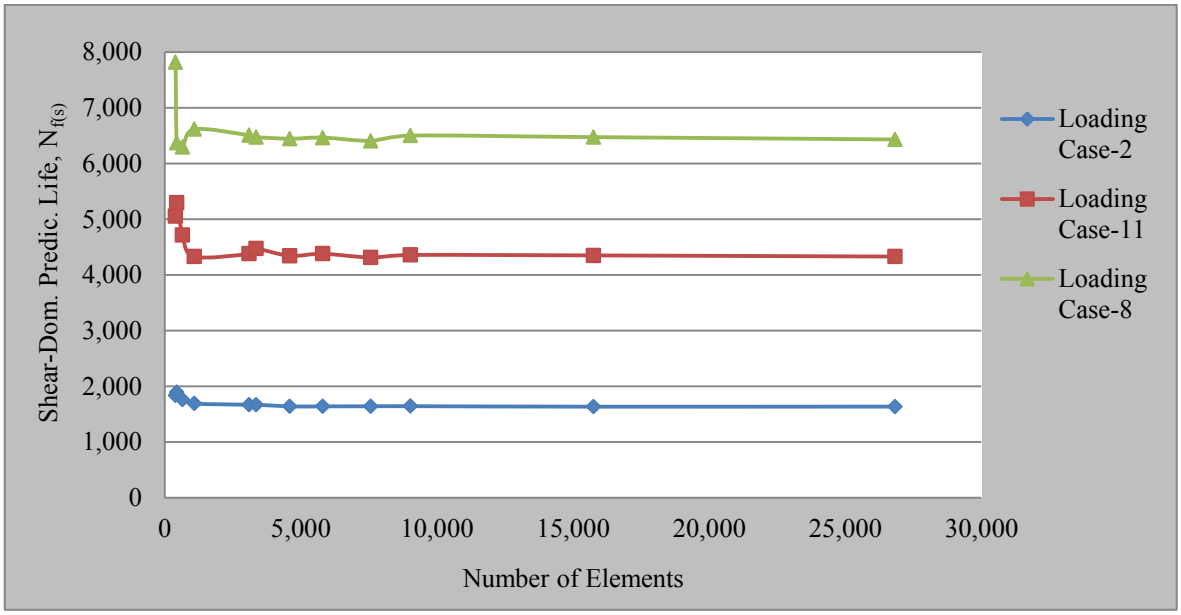

Figure 5.3. Mesh convergence for shear dominant predicted life, $N_{f(s)}$ of specimen-1.

Figure 5.4 gives the measured and predicted lives with increasing order of final fracture measured lives. One another way to present the comparison between the measured and predicted lives is a scale chart that shows the accurate predictions between some determined scales. Figure 5.5 gives the prediction scale chart of specimen-1 with a scale limits between 0.5-2.0 and 0.33-3.0. It shows that for 20 of 37 loading cases, shear dominant fatigue model predicts the fatigue life with a prediction scale between 0.33-3.0.

Most damaging case for specimen-1 is the loading case-1 for which a life of only 1,802 cycles is predicted. The corresponding strain energy density contour is in Figure 5.6.

Table 5.2. The model prediction results and the fatigue lives reported by [53].

Loading Case	Applied Bending Moment (N.m)	Applied Torsional Moment (N.m)	Eqv. Strain Energy Density Amplitude, U_a (Pa) (for axial)	Eqv. Strain Energy Density Amplitude, U_a (Pa) (for shear)	Crack Initiation Life, $N_{f(exp)}(i)$	Final Fracture Life, $N_{f(exp)}(f)$	Axial-Dominant Predicted Life, $N_{f(a)}$	Shear-Dominant Predicted Life, $N_{f(s)}$
1	1,850	2,550	3.51E+05	3.30E+05	2,200	5,113	11,331	1,802
2	2,800	0	3.59E+05	3.35E+05	2,571	8,262	10,084	1,643
3	1,250	2,700	3.00E+05	3.54E+05	6,402	10,420	27,024	1,238
4	1,698	2,242	2.95E+05	2.73E+05	6,725	10,840	29,422	4,724
5	1,355	2,550	2.90E+05	2.69E+05	5,500	11,630	32,358	5,125
6	2,325	1,350	3.12E+05	2.89E+05	2,905	11,735	21,461	3,523
7	2,000	2,100	3.23E+05	3.00E+05	5,998	12,050	17,782	2,937
8	0	3,000	2.78E+05	2.57E+05	5,529	12,124	40,489	6,503
9	1,150	2,700	2.89E+05	2.68E+05	6,800	12,900	32,887	5,181
10	2,600	0	3.19E+05	2.95E+05	6,347	15,043	19,327	3,199
11	1,850	2,100	3.01E+05	2.78E+05	8,047	16,867	26,204	4,359
12	2,586	0	3.16E+05	2.93E+05	14,000	17,450	20,348	3,322
13	851	2,700	2.67E+05	2.45E+05	9,000	17,730	50,249	8,377
14	2,300	1,325	3.06E+05	2.83E+05	17,720	23,980	24,054	3,936
15	840	2,700	2.66E+05	2.44E+05	10,000	24,540	51,185	8,525
16	1,800	2,100	2.93E+05	2.72E+05	21,600	24,620	30,215	4,888
17	1,295	1,710	2.00E+05	1.74E+05	25,580	45,800	239,719	47,859
18	1,720	1,350	2.21E+05	1.96E+05	19,260	58,790	139,439	26,078
19	1,680	960	1.97E+05	1.70E+05	30,000	65,049	264,904	54,507
20	1,875	0	1.97E+05	1.72E+05	48,180	112,200	261,660	51,516
21	1,220	1,700	1.93E+05	1.67E+05	60,800	124,500	293,815	60,337
22	0	2,400	2.00E+05	1.78E+05	70,350	132,585	243,909	43,733
23	1,680	900	1.94E+05	1.67E+05	84,950	153,800	288,612	59,935
24	780	2,180	2.02E+05	1.78E+05	70,340	156,100	231,444	43,270
25	770	2,180	2.02E+05	1.77E+05	151,900	157,100	229,274	44,198
26	1,730	0	1.81E+05	1.52E+05	67,300	157,125	412,180	97,288
27	570	2,180	1.92E+05	1.67E+05	87,830	182,250	302,559	60,613
28	1,550	1,090	1.88E+05	1.61E+05	88,750	190,200	336,142	72,512
29	1,220	1,710	1.94E+05	1.68E+05	127,575	200,450	285,929	58,457
30	1,300	1,400	1.81E+05	1.53E+05	84,680	226,000	416,355	95,082
31	1,708	0	1.79E+05	1.50E+05	163,800	249,900	437,498	103,733
32	845	1,800	1.75E+05	1.45E+05	259,900	396,800	498,872	125,635
33	1,475	0	2.10E+05	1.22E+05	347,500	556,400	187,096	298,887
34	1,250	880	2.00E+05	1.20E+05	462,500	734,750	240,609	330,748
35	1,460	0	2.06E+05	1.22E+05	430,000	764,000	209,082	297,592
36	990	1,390	1.91E+05	1.25E+05	641,500	890,500	311,560	263,129
37	0	2,000	1.68E+05	1.35E+05	1,011,333	1,843,667	626,002	176,343

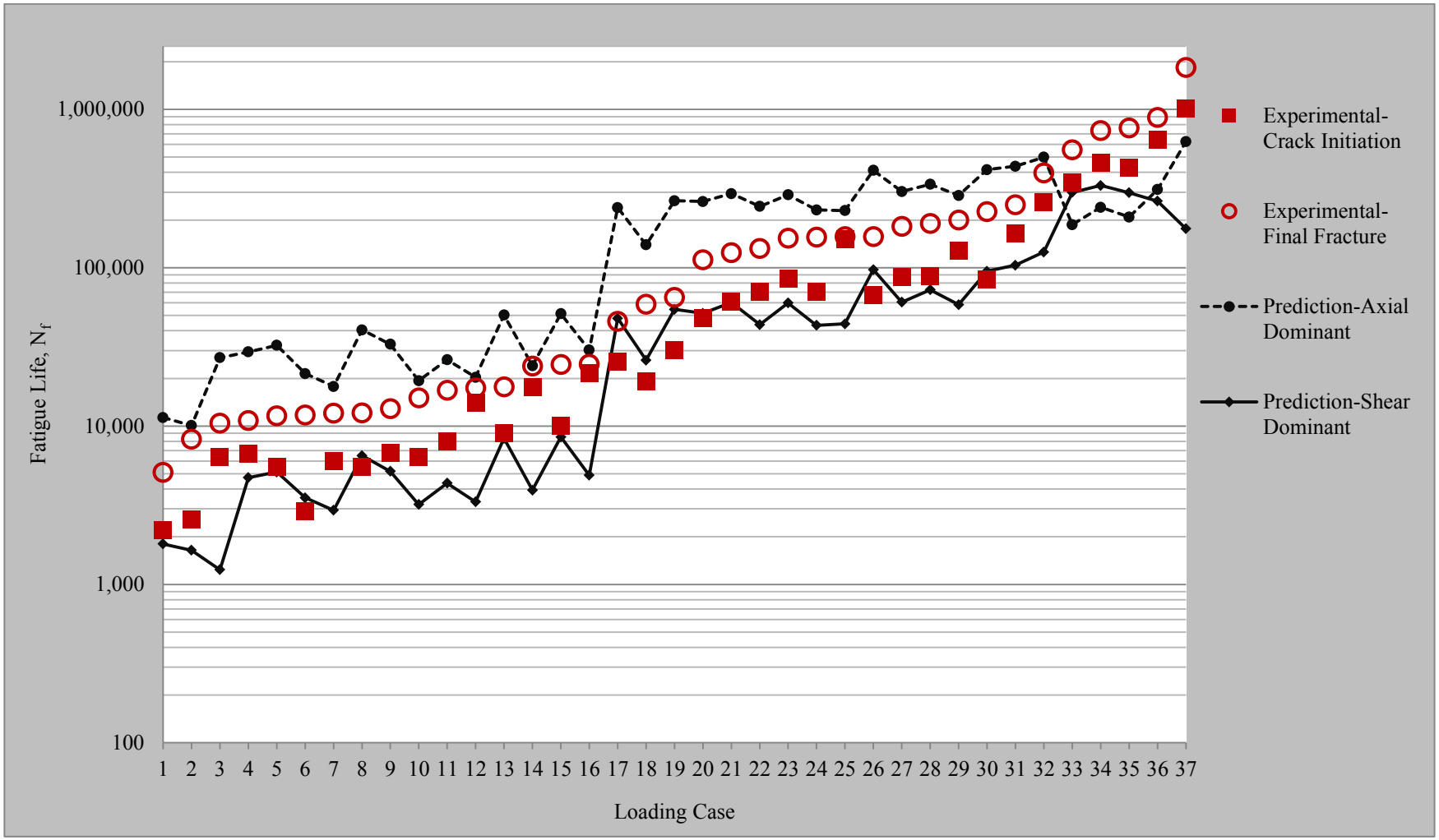

Figure 5.4. Comparison between the model predictions and the fatigue lives reported by [53].

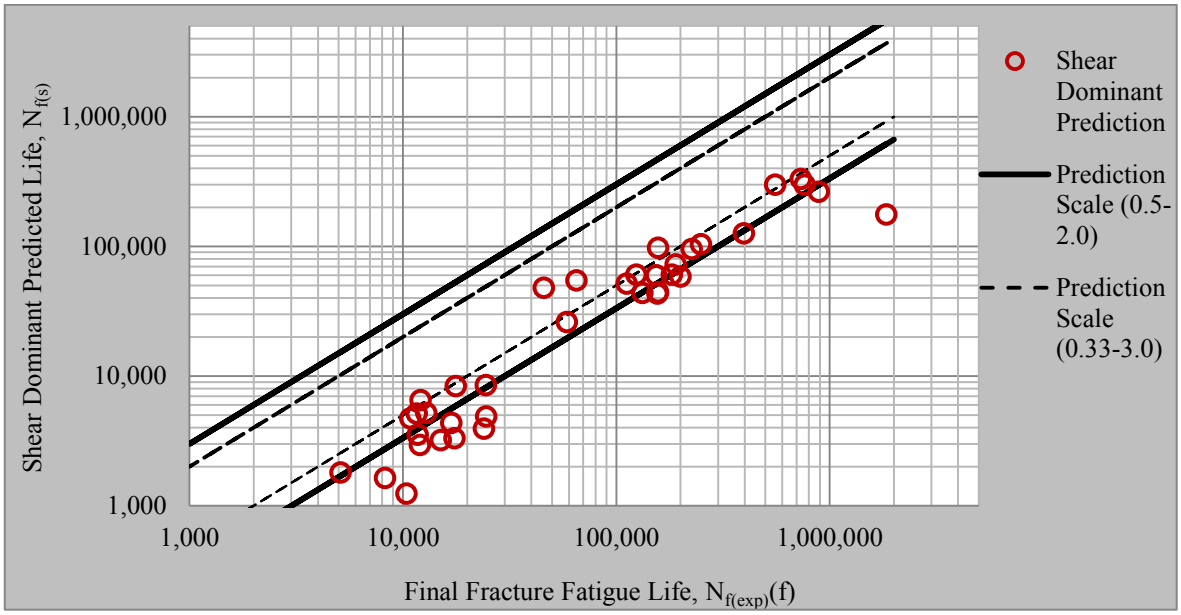

Figure 5.5. Prediction chart of specimen-1 with scale limits between 0.5-2.0 and 0.33-3.0.

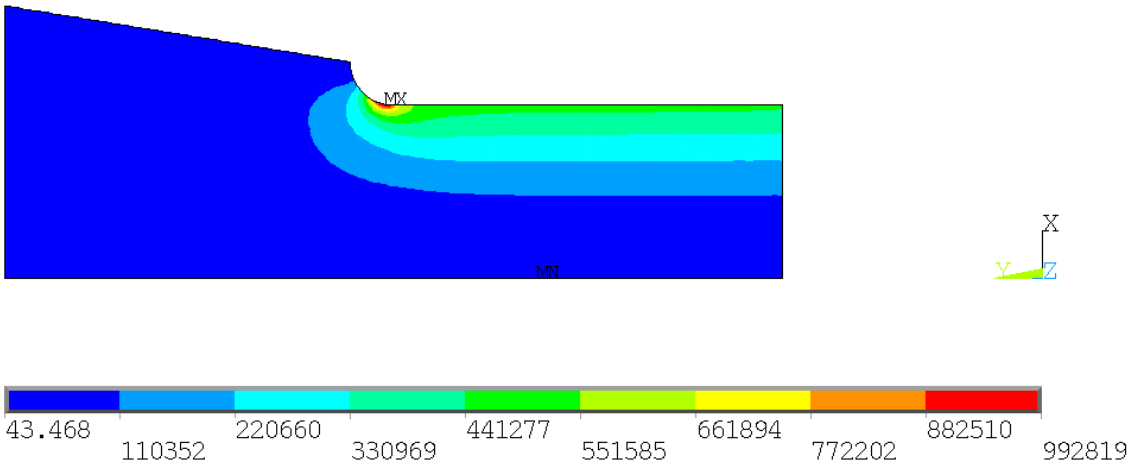

Figure 5.6. Strain energy density contour of loading case-1 for specimen-1. The dimensions are in pascals.

5.2. Comparative Results for Specimen-2

For specimen-2, Jen and Wang [54] provided only crack initiation lives. Final fracture case was expected to take at least two times longer than the crack initiation.

Before outlining the predicted life results, the calculation steps for the applied loads will be examined. The authors [54] gave only equivalent stress amplitudes, but not the

axial and torsional loads. Firstly, axial and shear nominal stress amplitudes are calculated using Equations 5.1 and 5.2 by make use of the given equivalent stress amplitude, $\sigma'_{nom,a}$, and biaxial nominal stress ratio, ϕ, which is defined as the ratio of axial nominal stress amplitude to the shear nominal stress amplitude.

$$\sigma'_{nom,a} = \sqrt{\sigma^2_{nom,a} + 3\tau^2_{nom,a}} \tag{5.1}$$

$$\phi = \sigma_{nom,a}/\tau_{nom,a} \tag{5.2}$$

After axial and shear nominal stresses are defined, axial and torsional loads are calculated. Axial loads are calculated for the 12-mm smooth diameter as in Figure 4.9. Torsional loads are calculated using Nadai's Equation [56] in Equation 5.3 which ends up with a more familiar form.

$$\tau = \frac{1}{2\pi r^3}(3T + \varphi\frac{dT}{d\varphi}) \tag{5.3}$$

where T is the applied torque, φ is twist angle per unit length and r is the radius of the smooth the specimen. However, this can be simplified in the following theorem.

Theorem 5.1. *Shear stress in Equation* 5.3 *can be simplified to Equation 5.4.*

$$\tau = \frac{Tc}{J} \tag{5.4}$$

Proof. The relation between torque and twist angle, θ, is used to write torque, T, in Equation 5.3.

$$\theta = \frac{TL}{GJ}$$

$$\varphi L = \frac{TL}{GJ}$$

$$\varphi = \frac{T}{GJ}$$

Rewriting Equation 5.3, it is simplified to

$$\tau = \frac{1}{2\pi r^3}(3T + \varphi \frac{dT}{d\varphi})$$

$$\tau = \frac{1}{2\pi r^3}(3T + \frac{T}{GJ}GJ)$$

$$\tau = \frac{2T}{\pi r^3}$$

$$\tau = \frac{Tr}{(\frac{\pi r^4}{2})}$$

$$\tau = \frac{Tc}{J}$$

where J is polar moment of inertia and c is the eccentricity where it is equal to radius for maximum stress value. Table 5.3 shows the list of applied loads. □

Table 5.4, Figure 5.7, Figure 5.8 and Figure 5.9 show mesh convergence of three loading case for equivalent strain energy density, maximum stress energy density and shear dominant fatigue life prediction, respectively. 127,899 elements are used where there is no significant change with further increase in element numbers.

Experiments were performed three times for each loading case. Table 5.5 gives the average of those three experimental results and the model predictions. The load cases are listed in the order of increasing equivalent nominal stress amplitude. Results for specimen-2 is represented graphically in Figure 5.10.

Table 5.3. Applied loads for AISI 316 notched cylinder specimen.

Loading Case	Biaxial Nominal Stress Ratio, ϕ ($\sigma_{nom,a}/\tau_{nom,a}$)	Equivalent Nominal Stress Amplitude, $\sigma'_{nom,a}$ (MPa)	Axial Nominal Stress Amplitude, $\sigma_{nom,a}$ (MPa)	Shear Nominal Stress Amplitude, $\tau_{nom,a}$ (MPa)	Applied Axial Load (N)	Applied Torque (N.m)	Applied Shear Load Couple (N)
1	0	160	0	92.38	0	31,342	2,612
2	0	180	0	103.92	0	35,260	2,938
3	0	200	0	115.47	0	39,178	3,265
4	1/2	210	58.24	116.49	6,587	39,523	3,294
5	1/2	220	61.02	122.03	6,901	41,405	3,450
6	1/2	250	69.34	138.68	7,842	47,051	3,921
7	2	280	211.66	105.83	23,938	35,907	2,992
8	2	300	226.78	113.39	25,648	38,472	3,206
9	2	330	249.46	124.73	28,213	42,319	3,527
10	∞	280	280.00	0	31,667	0	0
11	∞	300	300.00	0	33,929	0	0
12	∞	330	330.00	0	37,322	0	0

Table 5.4. Mesh convergence of specimen-2.

Loading Case	Axial Nominal Stress Amplitude (MPa)	Shear Nominal Stress Amplitude (MPa)	Number of Elements	Eqv. Strain Energy Density, U_{eqv} (Pa) (for shear)	Max. Strain Energy Density, U_{max} (Pa) (for shear)	Shear-Dominant Predicted Life, $N_{f(s)}$
3	0.00	115.47	3,336	2.73E+05	4.41E+05	215,158
3	0.00	115.47	12,413	3.08E+05	5.11E+05	64,964
3	0.00	115.47	16,259	2.69E+05	5.68E+05	249,858
3	0.00	115.47	20,009	2.70E+05	5.58E+05	239,542
3	0.00	115.47	28,607	2.63E+05	5.21E+05	316,020
3	0.00	115.47	35,953	2.78E+05	5.46E+05	184,064
3	0.00	115.47	40,266	2.70E+05	5.42E+05	238,852
3	0.00	115.47	45,286	2.79E+05	5.48E+05	176,980
3	0.00	115.47	74,114	2.72E+05	5.96E+05	222,998
3	0.00	115.47	82,266	2.79E+05	5.28E+05	174,927
3	0.00	115.47	127,899	2.89E+05	5.36E+05	123,667
3	0.00	115.47	193,964	2.91E+05	5.88E+05	114,909
6	69.34	138.68	3,336	3.18E+05	9.74E+05	46,980
6	69.34	138.68	12,413	3.37E+05	1.08E+06	26,670
6	69.34	138.68	16,259	3.10E+05	1.20E+06	60,813
6	69.34	138.68	20,009	3.06E+05	1.21E+06	68,961
6	69.34	138.68	28,607	3.07E+05	1.19E+06	66,883
6	69.34	138.68	35,953	3.12E+05	1.22E+06	57,918
6	69.34	138.68	40,266	3.07E+05	1.22E+06	67,768
6	69.34	138.68	45,286	3.09E+05	1.24E+06	62,999
6	69.34	138.68	74,114	3.01E+05	1.24E+06	81,104
6	69.34	138.68	82,266	3.29E+05	1.24E+06	33,304
6	69.34	138.68	127,899	3.34E+05	1.27E+06	28,687
6	69.34	138.68	193,964	3.28E+05	1.23E+06	35,027
10	280.00	0.00	3,336	4.51E+05	2.33E+06	1,433
10	280.00	0.00	12,413	3.66E+05	2.89E+06	11,743
10	280.00	0.00	16,259	4.31E+05	3.16E+06	2,253
10	280.00	0.00	20,009	4.33E+05	3.04E+06	2,182
10	280.00	0.00	28,607	4.15E+05	3.06E+06	3,317
10	280.00	0.00	35,953	4.38E+05	3.18E+06	1,944
10	280.00	0.00	40,266	4.12E+05	3.34E+06	3,541
10	280.00	0.00	45,286	4.26E+05	3.18E+06	2,520
10	280.00	0.00	74,114	4.06E+05	3.24E+06	4,077
10	280.00	0.00	82,266	4.76E+05	3.20E+06	846
10	280.00	0.00	127,899	4.79E+05	3.34E+06	779
10	280.00	0.00	193,964	4.72E+05	3.24E+06	912

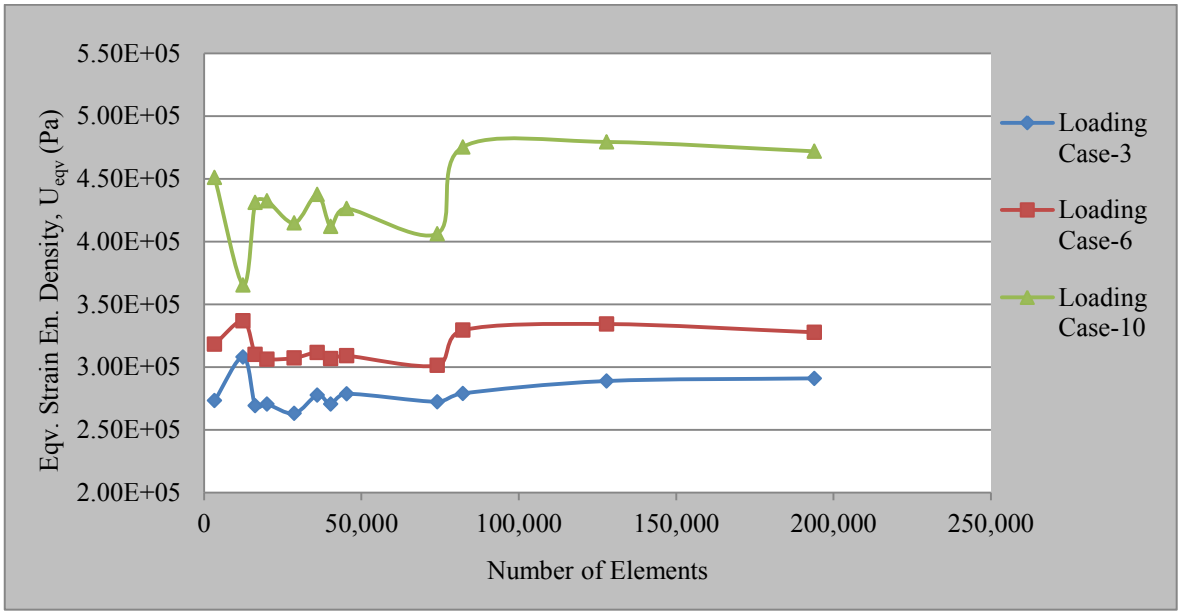

Figure 5.7. Mesh convergence for equivalent strain energy density, U_{eqv} of specimen-2.

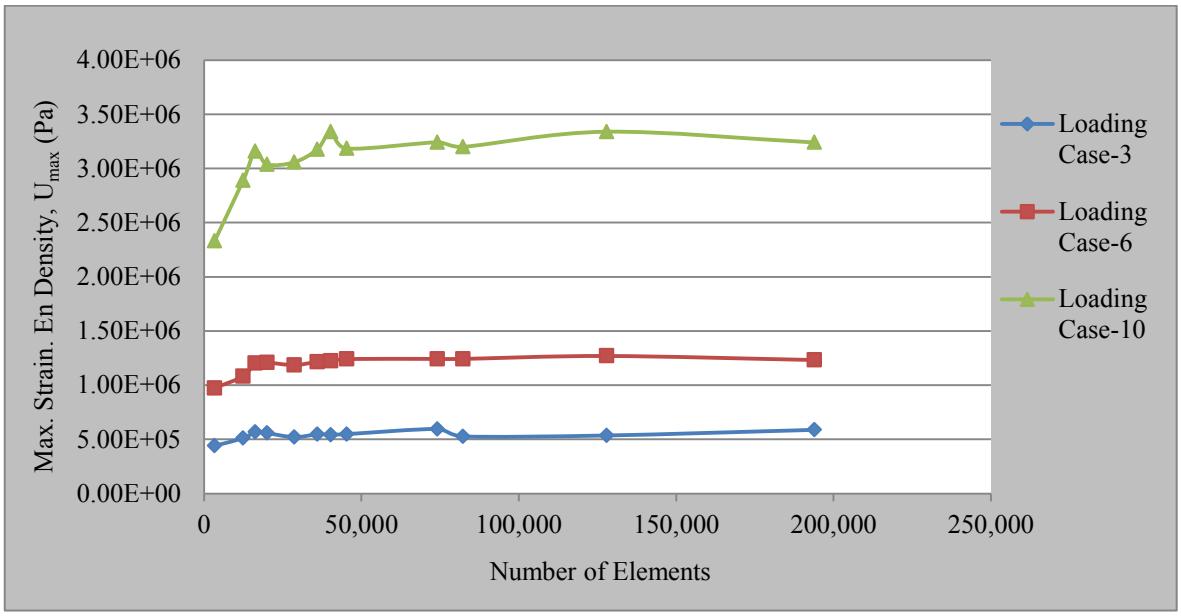

Figure 5.8. Mesh convergence for maximum strain energy density, U_{max} of specimen-2.

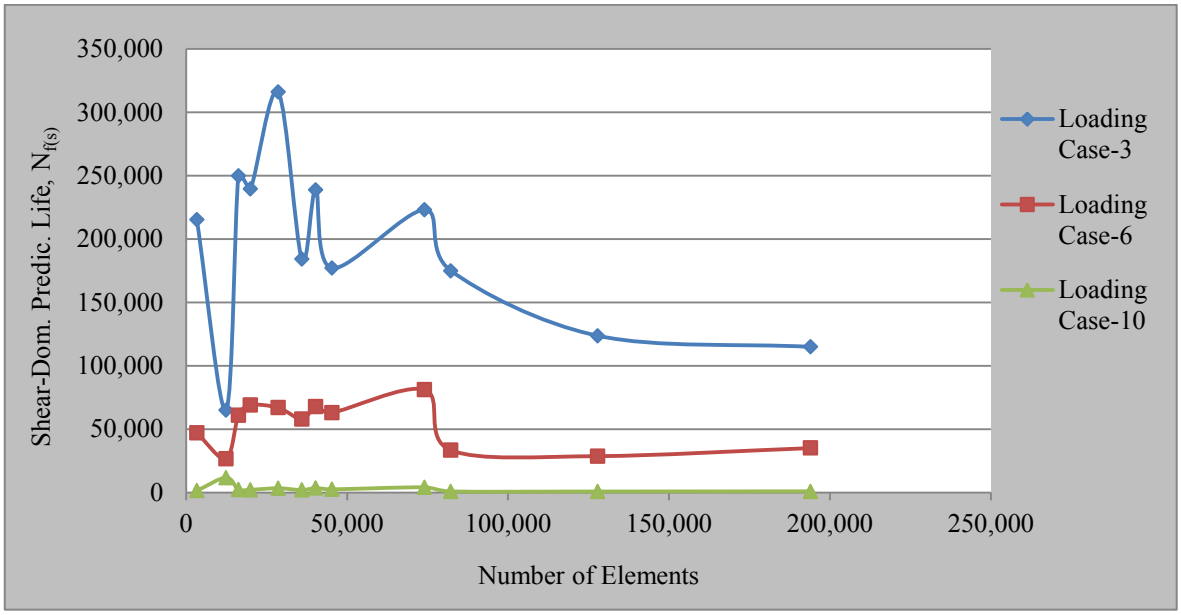

Figure 5.9. Mesh convergence for shear dominant predicted life, $N_{f(s)}$ of specimen-2.

The results show that proposed model is successful to predict the fatigue life except for the first three loading cases, where the applied loads are relatively lower. However, considering that the difference between crack initiation and final fracture lives is larger at lower levels of loads, the discrepancy between the predicted and actual final fracture lives is expected to be smaller. This also explains the discrepancy between the measured and predicted trends. One should also note that the experimental results showing no significant change in the fatigue lives while loads are getting larger are against intuition. For example, crack initiation life seems to be nearly equal for the loading cases 1 and 10, where equivalent nominal stresses are 160 and 220 MPa, respectively. This can be a result of the fact that the experimental results are the ones of crack initiation, not final fracture. Actually, for a better understanding it should be noted that final fracture life would be higher than crack initiation life where predicted results would be more accurate.

Axial dominant predictions are not as good as shear dominant results as in specimen-1. Figure 5.11 gives the prediction scale chart of specimen-2 with a scale limits between 0.5-2.0 and 0.33-3.0 again. It shows that for the half of loading cases, shear dominant fatigue model predicts the fatigue life with a prediction scale between 0.33-3.0.

Table 5.5. Fatigue life prediction results for specimen-2.

Loading Case	Axial Nominal Stress Amplitude (MPa)	Shear Nominal Stress Amplitude (MPa)	Applied Axial Load (N)	Applied Shear Load Couple (N)	Eqv. Strain Energy Density Amplitude, U_a (Pa) (for axial)	Eqv. Strain Energy Density Amplitude, U_a (Pa) (for shear)	Crack Initiation Life, $N_{f(exp)}(i)$	Axial-Dominant Predicted Life, $N_{f(a)}$	Shear-Dominant Predicted Life, $N_{f(s)}$
1	0.00	92.38	0	2,612	2.76E+05	2.69E+05	10,795	557,398	255,551
2	0.00	103.92	0	2,938	2.99E+05	2.83E+05	4,124	367,976	150,138
3	0.00	115.47	0	3,265	3.04E+05	2.89E+05	1,270	334,423	123,667
4	58.24	116.49	6,587	3,294	3.46E+05	3.32E+05	13,345	174,165	30,972
5	61.02	122.03	6,901	3,450	3.44E+05	3.23E+05	9,878	177,215	40,195
6	69.34	138.68	7,842	3,921	3.47E+05	3.34E+05	2,652	169,158	28,687
7	211.66	105.83	23,938	2,992	4.01E+05	3.89E+05	17,443	81,299	6,366
8	226.78	113.39	25,648	3,206	4.27E+05	4.16E+05	7,795	58,670	3,223
9	249.46	124.73	28,213	3,527	4.49E+05	4.30E+05	3,205	45,254	2,311
10	280.00	0.00	31,667	0	4.95E+05	4.79E+05	8,575	27,368	779
11	300.00	0.00	33,929	0	5.07E+05	4.52E+05	3,843	24,153	1,400
12	330.00	0.00	37,322	0	4.84E+05	4.79E+05	735	30,664	792

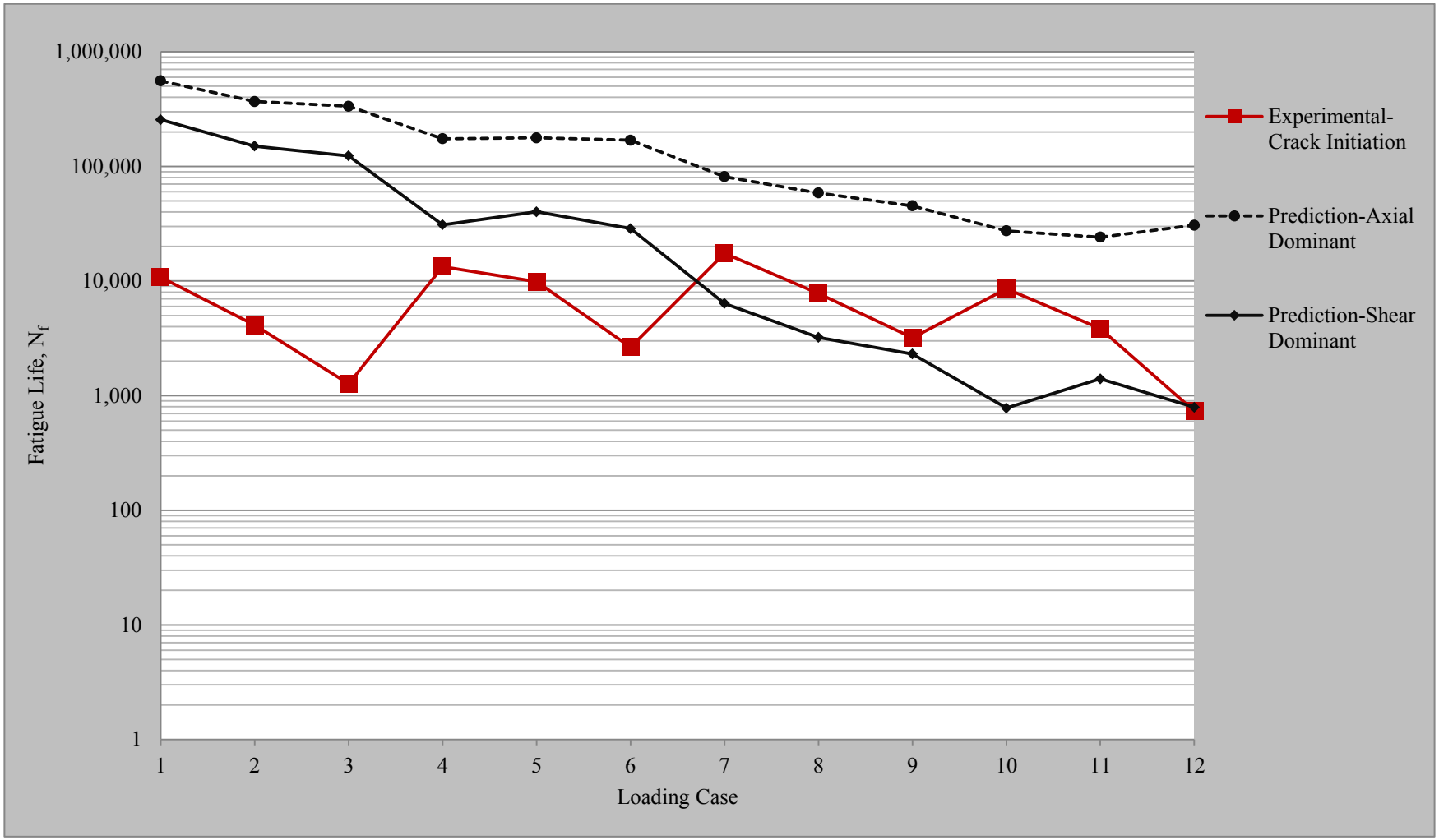

Figure 5.10. Comparison between the model predictions and the fatigue lives reported by [54].

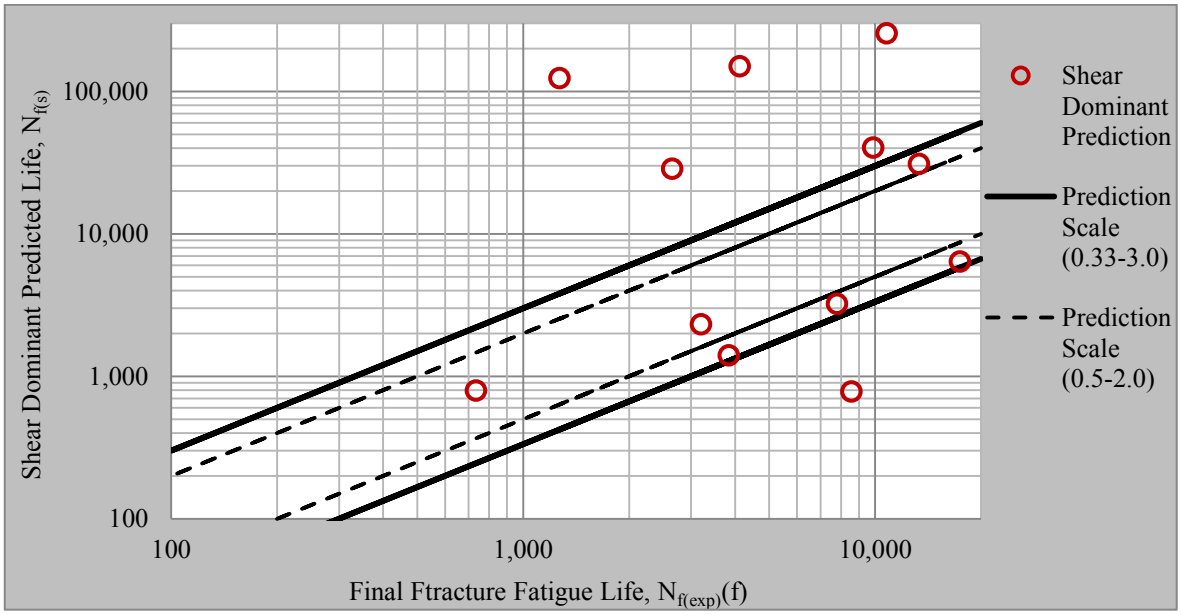

Figure 5.11. Prediction chart of specimen-2 with scale limits between 0.5-2.0 and 0.33-3.0.

For a better comparison, Figure 5.12 shows the comparison of experimental and proposed predicted results with the ones of eight other fatigue models which are stated in [16, 57-63]. For the last eight of twelve studies, the results of shear dominant model prediction is competitive. Also for those, the proposed shear dominant model underpredicts the fatigue life comparing with the most of the other models. The reason for that is the proposed model takes the contribution of a critical region in the part where the finite elements have a fatigue life lower than 106 where the other models calculate the fatigue life in the maximum deformed or maximum stressed point.

Additionally, Figure 5.13 shows the strain energy density contour of loading case-12 for shear dominant fatigue life prediction where it is the minimum of entire study for specimen-2.

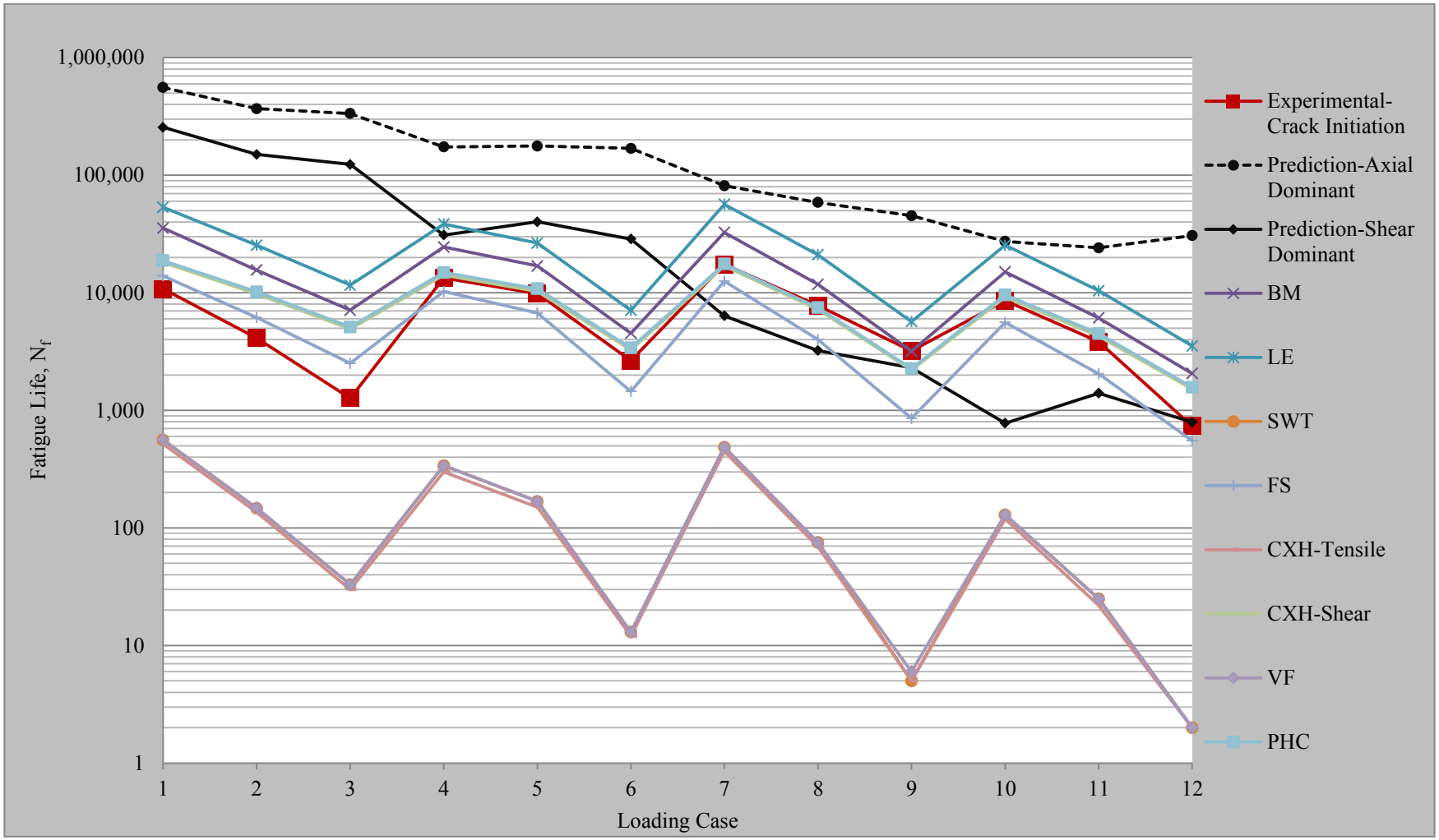

Figure 5.12. Comparison of fatigue life predictions for specimen-2.

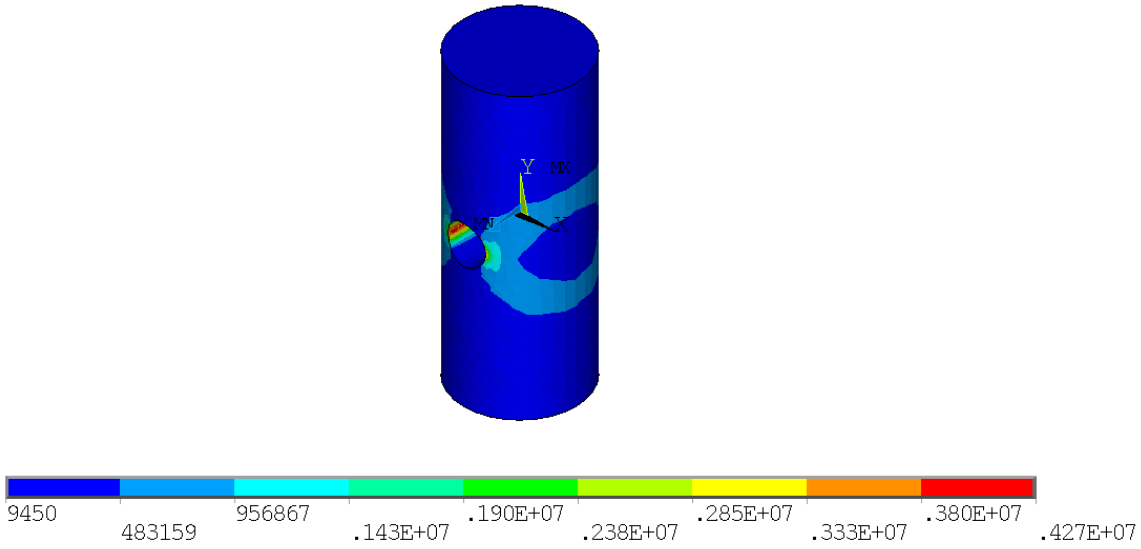

Figure 5.13. Strain energy density contour of loading case-12 for specimen-2. The dimensions are in pascals.

6. CONCLUSION

In this study, a new strain energy based fatigue model is proposed. The proposed model is developed to predict high cycle fatigue behavior of parts having notches or any stress raiser subjected to multiaxial loading. This covers most of the cases in industrial applications. The model includes only material parameters, which do not depend on geometry or loading conditions. The form of the model is based on Coffin-Manson-Basquin model. A new parameter is introduced called equivalent strain energy density. Its value is computed based on the strain energy density distribution within the part obtained via FEM. Because the model is developed for proportional loading, performing just a single finite element analysis is sufficient to calculate related strain energy density amplitudes and the corresponding fatigue life. Only the contributions of the finite elements that have fatigue life lower than 10^6 cycles are considered. The degree of the contribution of these elements depends on their strain energy density. In the formulation of equivalent strain energy density, the contribution of highly stressed elements are biased.

The model predictions are compared with the results of two experimental studies. In those studies, two different steel materials were used, SAE 1045 carbon steel and AISI 316 stainless steel; the specimens contained two different notches, one was a fillet the other was a circular hole. The specimens were subjected to different types of multiaxial loading, one was bending moment combined with torsion, the other was axial loading combined with torsion. Specimens were tested for many different combinations of load levels. Comparisons were made for 49 different testing conditions.

Considering the large scatter in the empirical fatigue data, predictions are found to be quite acceptable, especially for those obtained using shear dominant fatigue coefficients. The reason of the fact that the model with shear dominant fatigue coefficients predicts the fatigue life better than the one with axial dominant fatigue coefficients is highly probable that the multiaxial fatigue failure is dominated by the shear strains.

APPENDIX A: ALTERNATIVE FORMULATION OF EQUIVALENT STRAIN ENERGY DENSITY

In Section 3.1, the contribution of the finite elements are formulized with the characteristic part of the Coffin-Manson-Basquin equation, $(2N_f^k)^{2b}$ for axial dominant predicted model and $(2N_f^k)^{2b'}$ for shear dominant predicted model. The other idea might be to use the derivative of the characteristic part in the formulation of the equivalent strain energy density. This leads to

$$U_{ea} = \frac{\sum_{k=1}^{n} V_k (2N_f^k)^{2b-1} U_a^k}{\sum_{k=1}^{n} V_k (2N_f^k)^{2b-1}} \tag{A.1}$$

where the multiplier $2b - 1$ is excluded because it is constant for all contributing elements. Axial dominant fatigue coefficients and exponents should be replaced with shear dominant fatigue coefficient and exponents for shear dominant model prediction. The predicted results for specimen-1 are shown in Figure A.1 with the experimental results.

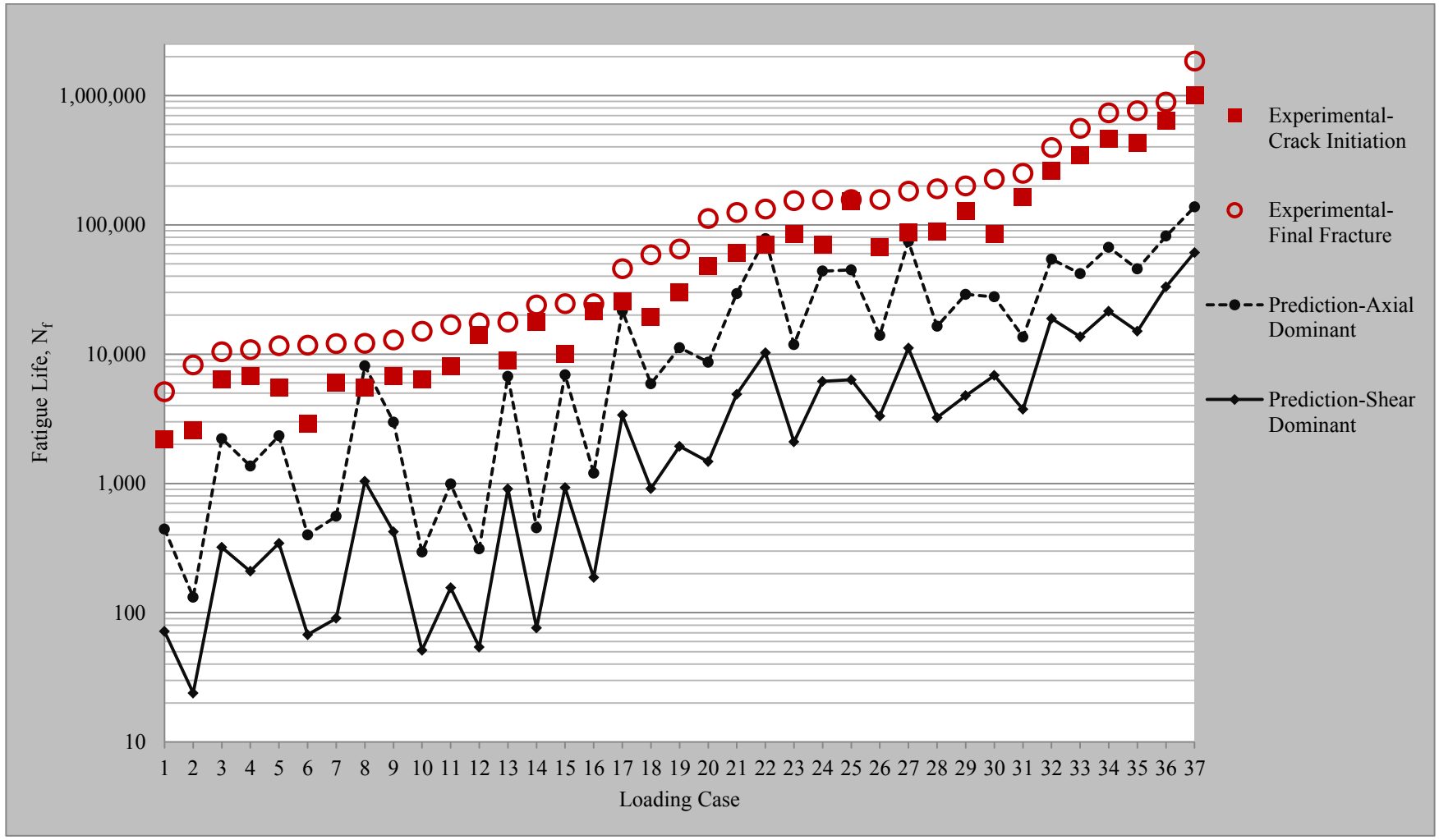

Figure A.1. Comparison between the alternative model predictions and the fatigue lives reported by [53].

REFERENCES

1. Susmel, L. and D. Taylor, "The Modified Wöhler Curve Method Applied Along with the Theory of Critical Distances to Estimate Finite Life of Notched Components Subjected to Complex Multiaxial Loading Paths", *Fatigue & Fracture of Engineering Materials & Structure*, Vol. 31, No. 12, pp. 1047–1064, 2008.

2. Ranganathan, N., H. Aldroe, F. Lacroix, F. Chalon, R. Leroy and A. Tougui, "Fatigue Crack Initiation at a Notch", *International Journal of Fatigue*, Vol. 33, No. 3, pp. 492–499, 2011.

3. Chaudonneret, M., and J. L. Chaboche, "Fatigue Life Prediction of Notched Specimens", *International Conference on Fatigue of Engineering Materials and Structures*, 1986, Sheffield.

4. Giancane, S., R. Nobile, F. W. Panella and V. Dattoma, "Fatigue Life Prediction of Notched Components Based on a New Nonlinear Continuum Damage Mechanics Model", *Procedia Engineering*, Vol. 2, No. 1, pp. 1317-1325, 2010.

5. Rashed, G., R. Ghajar and S. J. Hashemi, "Evaluation of Multiaxial Fatigue Life Prediction Model Based on Critical Plane for Notched Specimens", *International Journal of Damage Mechanics*, Vol. 17, No. 5, pp. 419-445, 2008.

6. Carpinteri, A., A. Spagnoli, S. Vantadori and D. Viappiani, "A Multiaxial Criterion for Notch High-Cycle Fatigue Using a Critical-Point Method", *Engineering Fracture Mechanics*, 2008, Vol. 75, No. 7, pp. 1864–1874, 2008.

7. Capetta, S., R. Tovo, D. Taylor and P. Livieri, "Numerical Evaluation of Fatigue Strength on Mechanical Notched Components Under Multiaxial Loadings", *International Journal of Fatigue*, Vol. 33, No. 5, pp. 661–671, 2011.

8. Chaboche, J. L., “Continuum Damage Mechanics: Part I - General Concepts”, *Journal of Applied Mechanics*, *Transactions ASME*, Vol. 55, No. 1, pp. 59-64, 1988.

9. Chaboche, J. L., “Continuum Damage Mechanics: Part II - Damage Growth, Crack Initiation, and Crack Growth”, *Journal of Applied Mechanics*, *Transactions ASME*, Vol. 55, No. 1, pp. 65-72, 1988.

10. Marco, S. M. and W. L. Starkey, “A Concept of Fatigue Damage”, *Transactions ASME*, Vol. 76, No. 4, pp. 627-632, 1954.

11. Manson, S. S., “Some Useful Concept for the Designer in Treating Cumulative Damage at Elevated Temperature”, *Computer Networking Symposium 1*, 1979, Proceedings of the Third International Conference, Cambridge, pp. 13-45.

12. Xiao, Y. C., S. Li and Z. Gao, “A Continuum Damage Mechanics Model for High Cycle Fatigue”, *International Journal of Fatigue*, Vol. 20, No. 7, pp. 503-508, 1988.

13. Dattoma, V., S. Giancane, R. Nobile and F. W. Panella, “Fatigue Life Prediction Under Variable Loading Based on a New Non-Linear Continuum Damage Mechanics Model”, *International Journal of Fatigue*, Vol. 28, No. 2, pp. 89-95, 2006.

14. Shang, D. G. and W. X. Yao, “A Nonlinear Damage Cumulative Model for Uniaxial Fatigue”, *International Journal of Fatigue*, Vol. 21, No. 2, pp. 187–194, 1999.

15. Chen, H., D. G. Shang, M. Bao, “Selection of Multiaxial Fatigue Damage Model Based on the Dominated Loading Modes”, *International Journal of Fatigue*, Vol. 33, No. 5, pp. 735-739, 2011.

16. Brown, M. W. and K. J. Miller, “A Theory for Fatigue Failure Under Multiaxial Stress-Strain Conditions”, *Proceedings of the Institution of Mechanical Engineers*, Vol. 187, No. 65, pp. 745-755, 1973.

17. Ninic, D., "A Stress-Based Multiaxial High-Cycle Fatigue Damage Criterion", *International Journal of Fatigue*, Vol. 28, No. 2, pp. 103–113, 2006.

18. McDiarmid, D. L., "Fatigue under out-of-Phase Bending and Torsion", *Fatigue & Fracture of Engineering Materials & Structure*, Vol. 9, No. 6, pp. 457-475, 1987.

19. McDiarmid, D. L., *Failure Criteria and Cumulative Damage in Fatigue under Multi-Axial Stress Condition*, Ph.D. Thesis, The City University, London, 1972.

20. Carpinteri, A. and A. Spagnoli, "Multiaxial High-Cycle Fatigue Criterion for Hard Metals", *International Journal of Fatigue*, Vol. 23, No. 2, pp. 135-145, 2001.

21. Spagnoli, A., "A new High-Cycle Fatigue Criterion Applied to out-of-Phase Biaxial Stress State", *International Journal of Mechanical Sciences*, Vol. 43, No. 11, pp. 2581-2895, 2001.

22. Ninic, D. and H. L. Stark, "A Multiaxial Fatigue Damage Function", *International Journal of Fatigue*, Vol. 29, No. 3, pp. 533–548, 2007.

23. Gough H. J. and H. V. Pollard, "The Strength of Metals under Combined Alternating Stresses", *Proceedings of the Institution of Mechanical Engineers*, Vol. 131, pp. 1-103, 1935.

24. Liu, Y. and S. Mahadevan, "A Unified Multiaxial Fatigue Damage Model for Isotropic and Anisotropic Materials", *International Journal of Fatigue*, Vol. 29, No. 2, pp. 347–359, 2007.

25. Socie, D., "Critical Plane Approaches for Multiaxial Fatigue Damage Assessment", *Advances in Multiaxial Fatigue*, *ASTM STP*, Vol. 1191, ed. McDowell, D. L. and R. Ellis, *American Society for Testing and Materials*, pp. 7-36, 1993.

26. Fatemi, A. and L. Yang, "Cumulative Fatigue Damage and Life Prediction Theories: A Survey of the State of the Art for Homogeneous Materials", *International Journal of Fatigue*, Vol. 20, No. 1, pp. 9–34, 1998.

27. Miner, M. A., "Cumulative Damage in Fatigue", *Journal of Applied Mechanics*, Vol. 12, No. 3, pp. A159-A164, 1945.

28. Miller, K. J., "The Behavior of Short Fatigue Cracks and Their Initiation", In Mechanical Behavior of Materials—V, *Proceedings of the Fifth International Conference*, Vol. 1, ed. Yang, M. G., S. H. Zhang and Z. M. Zheng, pp. 1357-1381, 1987.

29. Leis, B. N., "A Nonlinear History-Dependent Damage Model for Low Cycle Fatigue", In Low Cycle Fatigue, *ASTM STP*, Vol. 942, ed. Solomon H. D., G. R. Halford, L. R. Kaisand and B. N. Leis, *American Society for Testing and Materials*, Philadelphia, PA, pp. 143-159, 1988.

30. Łagoda, T., "Energy Models for Fatigue Life Estimation under Uniaxial Random Loading. Part I: The Model Elaboration", *International Journal of Fatigue*, Vol. 23, No. 6, pp. 467-480, 2001.

31. Mrozinski, S. and S. M. Topolinski, "New Energy Model for Fatigue Damage Accumulation and Its Verification for 45-Steel", *Journal of Theoretical and Applied Mechanics*, Vol. 37, pp. 223-240, 1999.

32. Kaleta, J., *Experimental Bases of Formulation of the Energy Fatigue Hypotheses*, Scientific Papers of the Institute of Materials Science and Technical Mechanics of Technical University of Wroclaw 59, Series: Monographs, No. 24, Technical University of Wroclaw, Wroclaw, p. 144, 1998.

33. Łagoda, T., "Energy Models for Fatigue Life Estimation under Uniaxial Random Loading. Part II: Verification of the Model", *International Journal of Fatigue*, Vol. 23, No. 6, pp. 481-489, 2001.

34. Jahed, H. and A. Varvani-Farahani, "Upper and Lower Fatigue Life Limits Model Using Energy-Based Fatigue Properties", *International Journal of Fatigue*, Vol. 28, No. 5-6, pp. 467-473, 2006.

35. Ozaltun, H., M. H. H. Shen, T. George and C. Cross, "An Energy Based Fatigue Life Prediction Framework for In-Service Structural Components, *Experimental Mechanics*, Vol. 51, No. 5, pp. 707-718, 2011.

36. Gasiak, G. and R. Pawliczek, "Application of an Energy Model for Fatigue Life Prediction of Construction Steels under Bending, Torsion and Synchronous Bending and Torsion", *International Journal of Fatigue*, Vol. 25, No. 12, pp. 1339-1346, 2003.

37. Peeker, E. and E. Niemi, "Fatigue Crack Propagation Model Based on a Local Strain Approach", *Journal of Constructional Steel Research*, Vol. 49, No. 2, pp. 139-155, 1999.

38. Panasyuk, V. V. and V. P. Sylovanyuk, "A Computational Model of Fatigue Fracture of Materials", *Materials Science*, Vol. 39, No. 3, pp. 351-364, 2003.

39. Yuen, B. K. C. and F. Taheri, "Proposed Modification to the Zheng and Hirt Fatigue Model", *Journal of Materials Engineering and Performance*, Vol. 13, No. 2, pp. 226-231, 2004.

40. Zheng, X. and M. A. Hirt, "Fatigue Crack Propagation in Steels", *Engineering Fracture Mechanics*, Vol. 18, No. 5, pp. 965-973, 1983.

41. Papadopoulos, I. V., P. Davoli, C. Gorla, M. Filippin and A. Bernasconi, "A Comparative Study of Multiaxial High-Cycle Fatigue Criteria For Metals", *International Journal of Fatigue*, Vol. 19, No. 3, pp. 219-235, 1997.

42. Papuga, J., "A Survey on Evaluating the Fatigue Limit under Multiaxial Loading", *International Journal of Fatigue*, Vol. 33, No. 2, pp. 153–165, 2011.

43. Vu, Q. H., D. Halm and Y. Nadot, "Multiaxial Fatigue Criterion for Complex Loading Based on Stress Invariants", *International Journal of Fatigue*, Vol. 32, No. 7, pp. 1004–1014, 2010.

44. Liu, Y. and S. Mahadevan, "Multiaxial High-Cycle Fatigue Criterion and Life Prediction for Metals", *International Journal of Fatigue*, Vol. 27, No. 7, pp. 790–800, 2005.

45. Li, B. and M. Freitas, "A Procedure for Fast Evaluation of High-Cycle Fatigue under Multiaxial Random Loading", *Journal of Mechanical Design*, Vol. 124, No. 3, pp. 558-563, 2002.

46. Cristofori, A., L. Susmel and R. Tovo, "A Stress Invariant Based Criterion to Estimate Fatigue Damage under Multiaxial Loading", *International Journal of Fatigue*, Vol. 30, No. 9, pp. 1646–1658, 2008.

47. Lazzarin, P. and L. Susmel, "A Stress-Based Method to Predict Lifetime under Multiaxial Fatigue Loadings", *Fatigue & Fracture of Engineering Materials & Structure*, Vol. 26, No. 12, pp. 1171-1187, 2003.

48. Cristofori, A. and R. Tovo, "An Invariant-Based Approach for High-Cycle Fatigue Calculation", *Fatigue & Fracture of Engineering Materials & Structure*, Vol. 32, No. 4, pp. 310–324, 2009.

49. Zenner, H., A. Simbürger and J. Liu, "On the Fatigue Limit of Ductile Metals under Complex Multiaxial Loading", *International Journal of Fatigue*, Vol. 22, No. 2, pp. 137–145, 2000.

50. Doudard, C., S. Calloch, P. Cugy, A. Galtier and F. Hilt, "A Probabilistic Two-Scale Model for High-Cycle Fatigue Life Predictions", *Fatigue & Fracture of Engineering Materials & Structure*, Vol. 28, No. 3, pp. 279–288, 2005.

51. Lee, Y-L, J. Pan, R. B. Hathaway and M. E. Barkey, *Fatigue Testing and Analysis*, Elsevier Inc., USA, 2005.

52. Juvinall, R. C. and K. M. Marshek, *Fundamentals of Machine Component Design*, 4ed, John Wiley & Sons Inc., Asia, 2006.

53. Firat, M., "A Numerical Analysis of Combined Bending-Torsion Fatigue of SAE Notched Shaft", *Finite Elements in Analysis and Design*, Vol. 54, pp. 16-27, 2012.

54. Jen, Y. M. and W. W. Wang, "Crack Initiation Life Prediction for Solid Cylinders with Transverse Circular Holes under in-Phase and out-of-Phase Multiaxial Loading", *International Journal of Fatigue*, Vol. 27, No. 5, pp. 527-539, 2005.

55. Bannantine, J. A., Observation of Tension and Torsion Fatigue Cracking Behavior and the Effect on Multiaxial Damage Correlations, A report of the Materials Engineering-Mechanical Behavior, University of Illinois at Urbana-Campaign, Urbana, 1986.

56. Nadai, A., *Theory of Flow and Fracture of Solids*, 2ed, McGraw-Hill Book Company Inc., USA, 1950.

57. Lohr, R. D. and E. G. Ellison, "A Simple Theory for Low-Cycle Multiaxial Fatigue", *Fatigue & Fracture of Engineering Materials & Structure*, Vol. 3, No. 1, pp. 1-17, 1980.

58. Smith, K. N., P. Watson and T. H. Topper, "Stress-Strain Function for the Fatigue of Metals", *JMLSA*, Vol. 5, No. 4, pp. 767-778, 1970.

59. A. Fatemi and D. F. Socie, "A Critical Plane Approach to Multiaxial Fatigue Damage Including out-of-Phase Loading, *Fatigue & Fracture of Engineering Materials & Structure*, Vol. 11, No. 3, pp. 149-165, 1988.

60. Chen, X., S. Xu and D. Huang, "Ciritical Plane-Strain Energy Density Criterion for Multiaxial Low-Cycle Fatigue Life Under Non-Proportional Loading", *Fatigue & Fracture of Engineering Materials & Structure*, Vol. 22, No. 8, pp. 679-686, 1999.

61. Han, C., X. Chen and K. S. Kim, "Evaluation of Multiaxial Fatigue Criteria under Irregular Loading", *International Journal of Fatigue*, Vol. 24, No. 9, pp. 913-922, 2002.

62. Varvani-Farahani, A., "A New Energy-Critical Plane Parameter for Fatigue Life Assessment of Various Metallic Materials Subjected to in-Phase and out-of-Phase Multiaxial Loading Conditions", *International Journal of Fatigue*, Vol. 22, No. 4, pp. 295-305, 2002.

63. Pan, W. F., C. Y. Hung and L. L. Chen, "Fatigue Life Estimation under Multiaxial Loading", *International Journal of Fatigue*, Vol. 21, No. 1, pp. 3-10, 1999.